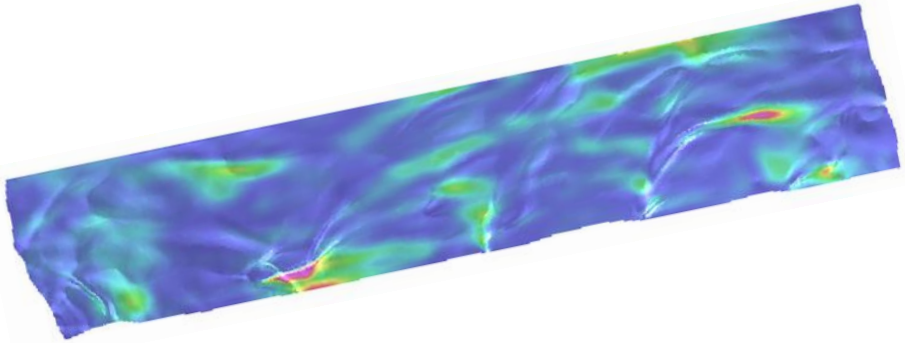

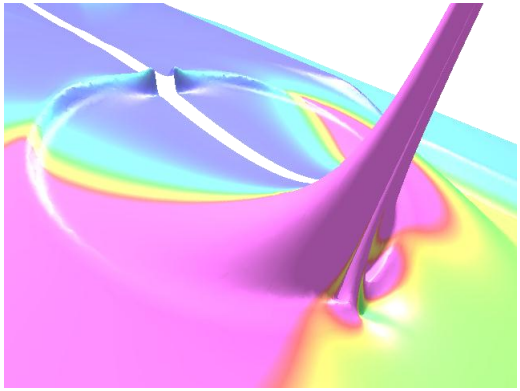

Theoretical and computational investigation of dynamic contact and fracture

Reza Abedi

Mechanical, Aerospace & Biomedical Engineering

University of Tennessee Knoxville / Space Institute

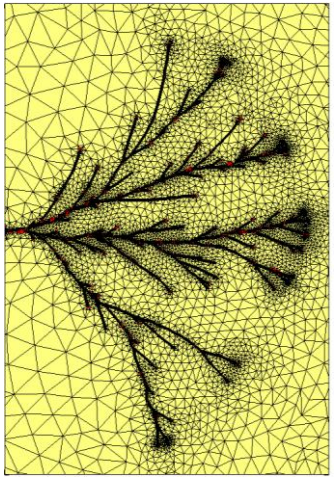

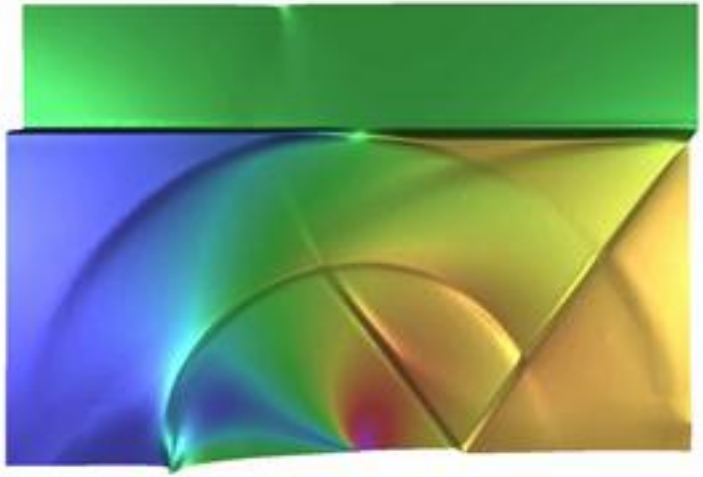

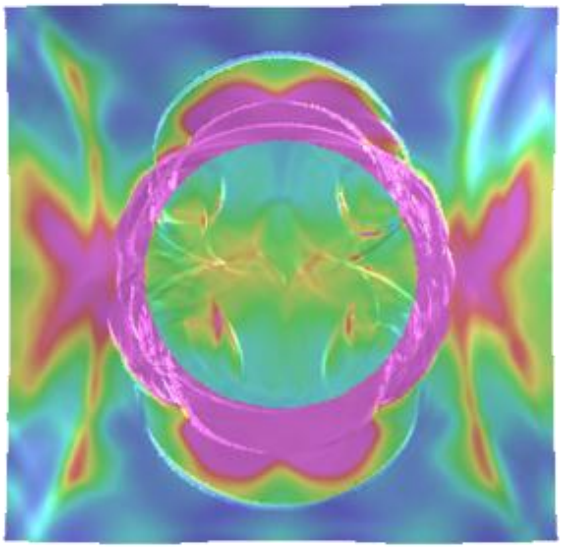

Part I:
Traction separation relations (TSRs) and Linear Elastic Fracture Mechanics (LEFM)

Cohesive models
Traction Separation Law

- Cohesive models remove stress singularity predicted by Linear Elastic Fracture Mechanics (LEFM)

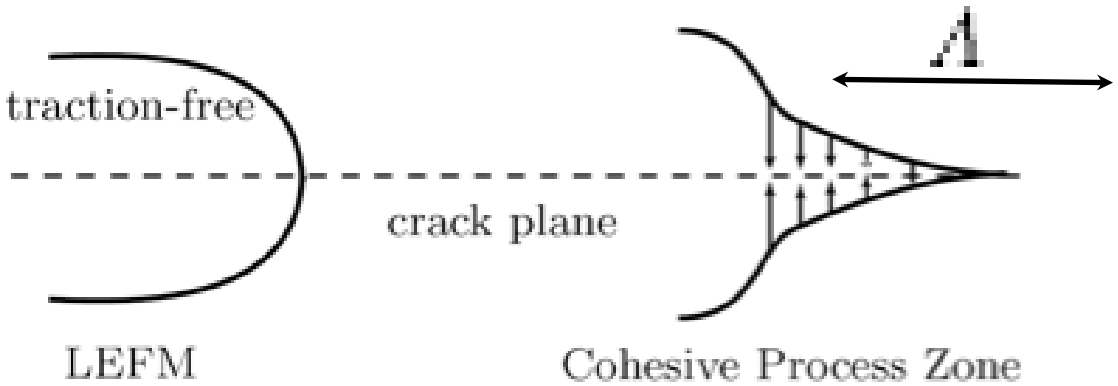

$\tilde{\sigma}$: Stress scale

$\tilde{\delta}$: Displacement scale

Λ: Length scale

$$\mathbf{s} \propto \frac{1}{\sqrt{r}}$$

$$\mathbf{s} = \tilde{\sigma}\mathbf{f}(\Delta\mathbf{u}/\tilde{\delta})$$

- Cohesive models are easily integrated into SDG method (discontinuous basis functions)

Cohesive Crack Propagation

click to play movie

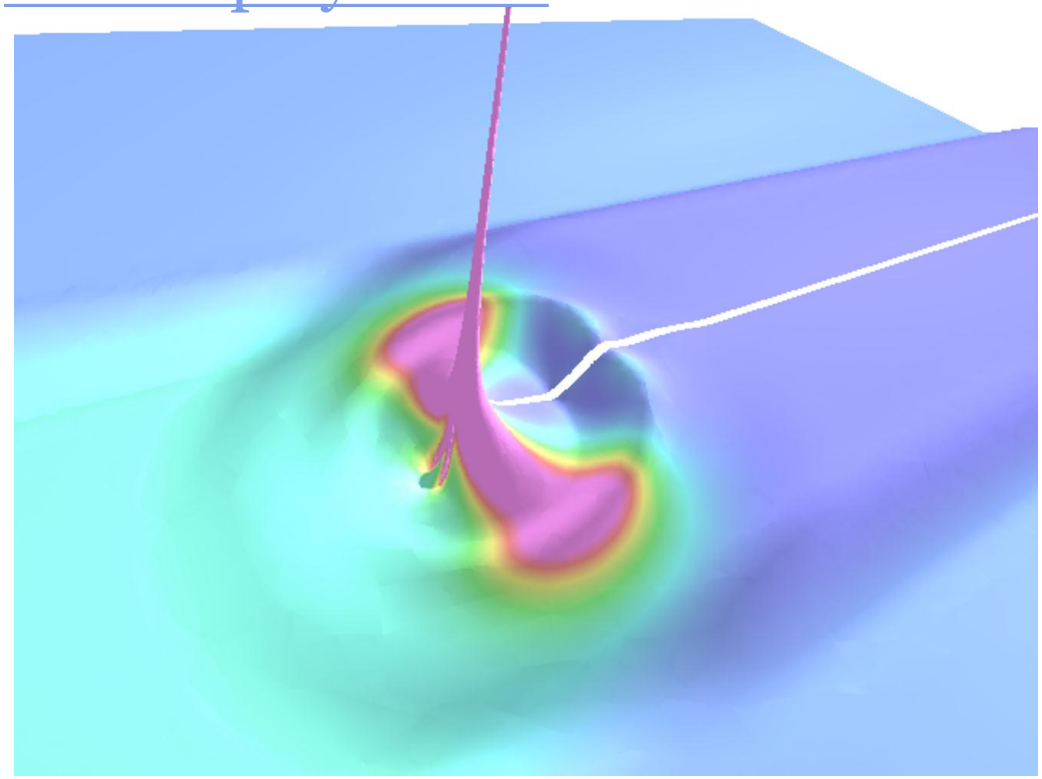

Color: log(strain energy); Height: velocity

Why does the spike form?

The velocity field is mapped to height field ⇨ high material velocities at the crack tip

Is the material velocity infinite at the crack tip (agreeing with LEFM theory)?

Cohesive Crack Propagation zoom view

click to play movie

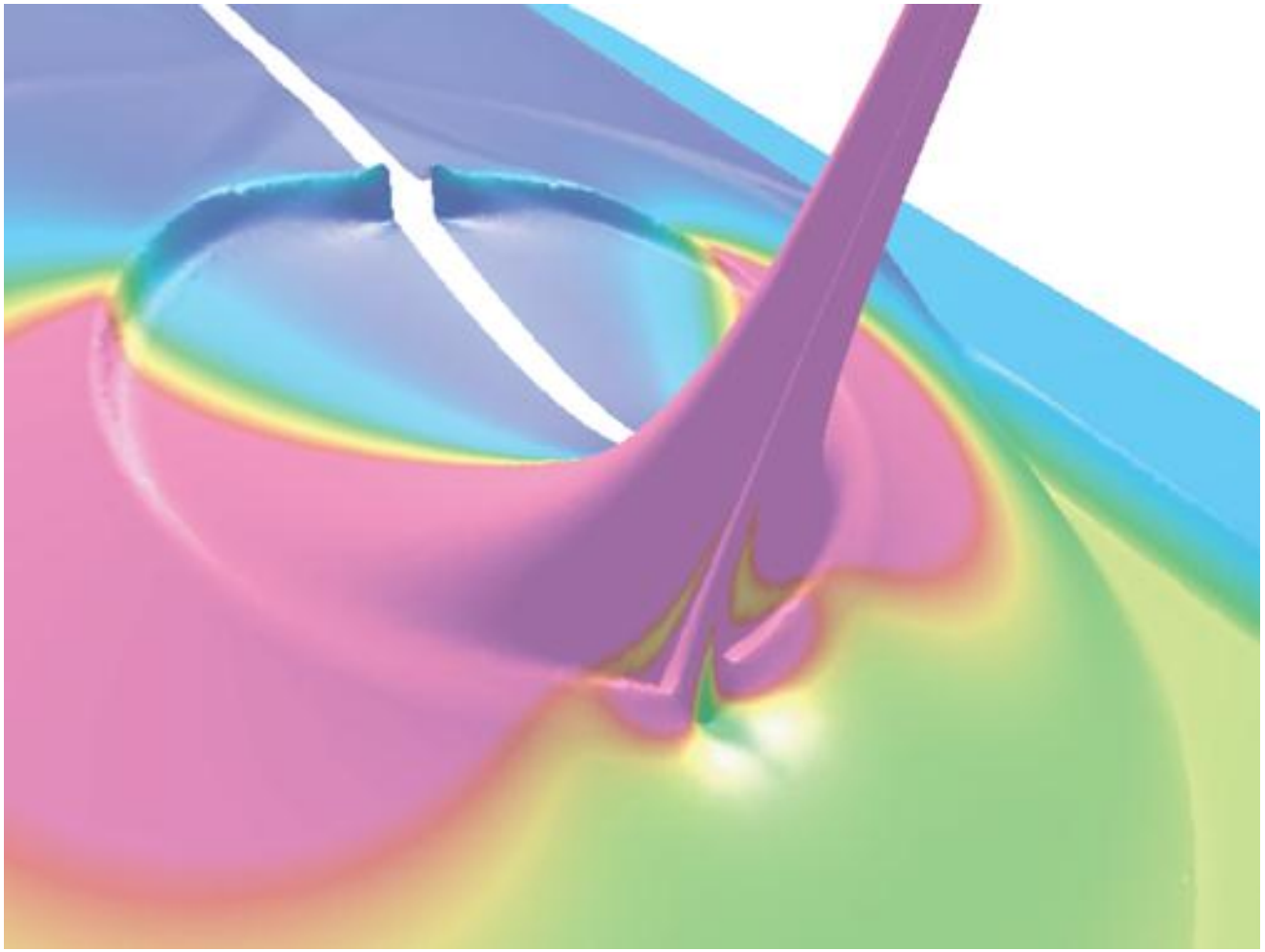

Color: log(strain energy); Height: velocity

Velocity-based length scales
LEFM vs. TSR

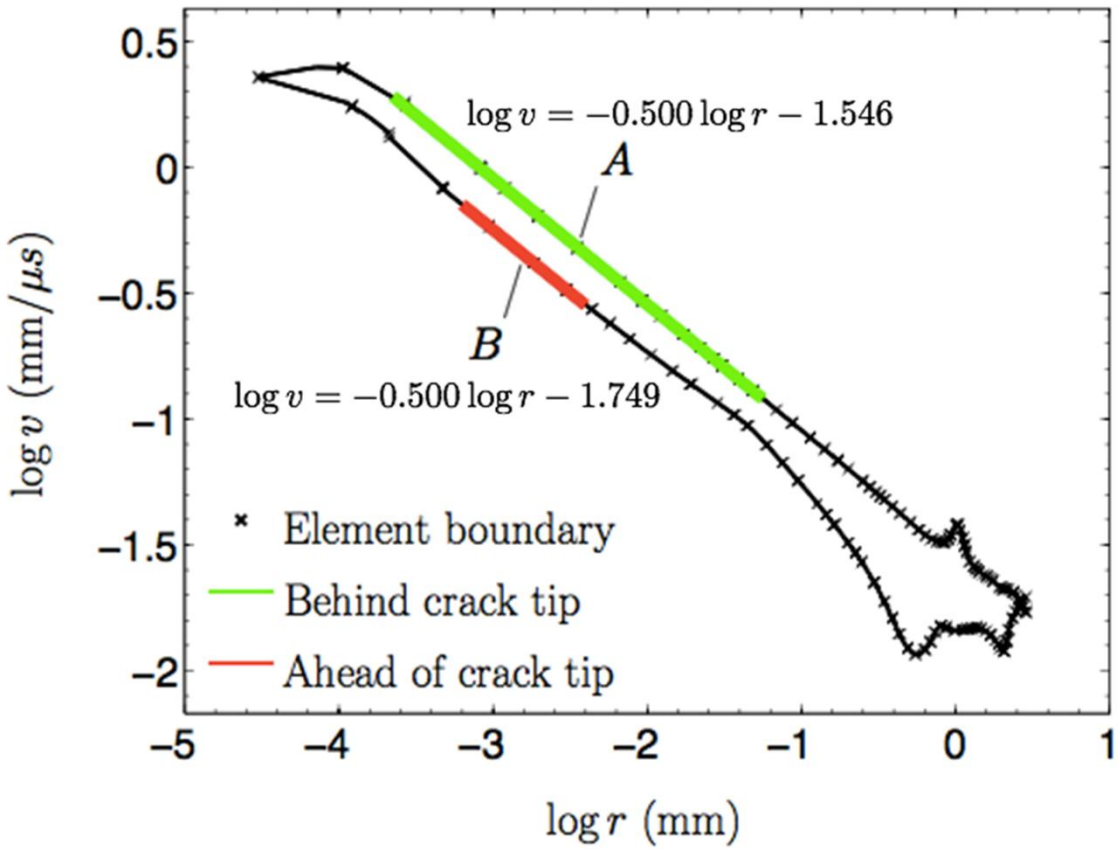

- LEFM length scale(singular radius)

r_v = size of the region where singular term dominates

- Cohesive length scale

Λ_v = plateau region size

Singular velocity response?

$$\frac{\Lambda_{v(k)}}{r_{v(k)}} = \beta_{(k)}\zeta_{(k)}\left(\frac{\pi c_2}{(1-\nu)c_k}\right)^2 \frac{\tilde{\phi}_{(k)}}{G}\left(\frac{\breve{\sigma}^k}{\tilde{\sigma}_{(k)}}\right)^2\left(A_{(k)}(\hat{v})\frac{\hat{v}}{c_2}\right)^{-2}$$

- Strongly sensitive to crack speed $\hat{v}$
  - $\Lambda_{v(k)}/r_{v(k)} \to \infty$ as $\hat{v} \to 0^+$
  - $\Lambda_{v(k)}/r_{v(k)} \to 0$ as $\hat{v} \to c_{\mathrm{R}}$
- Weak dependence on cohesive nondimensional parameter $\breve{\sigma}/\tilde{\sigma}$
- No evidence of "singular" response when $r_v < \Lambda_v$
- Follows singular form at positions $r \in [\Lambda_v, r_v]$ when $\Lambda_v \ll r_v$

Quasi-singular velocity response

$$\frac{|v_{(k)}|_\infty}{v_{\mathrm{C}k}} = \frac{1}{\sqrt{\gamma\beta_{(k)}\zeta_{(k)}}}\frac{(1-\nu)c_k}{\pi c_2}\left(\frac{G}{\tilde{\phi}_{(k)}}\right)^{\frac{1}{2}} A_{(k)}(\hat{v})\frac{\hat{v}}{c_2}$$

- $|v_{(k)}|_\infty$ bounded for all velocities.
- $|v_{(k)}|_\infty \to \infty$ as $\hat{v} \to c_{\mathrm{R}}$

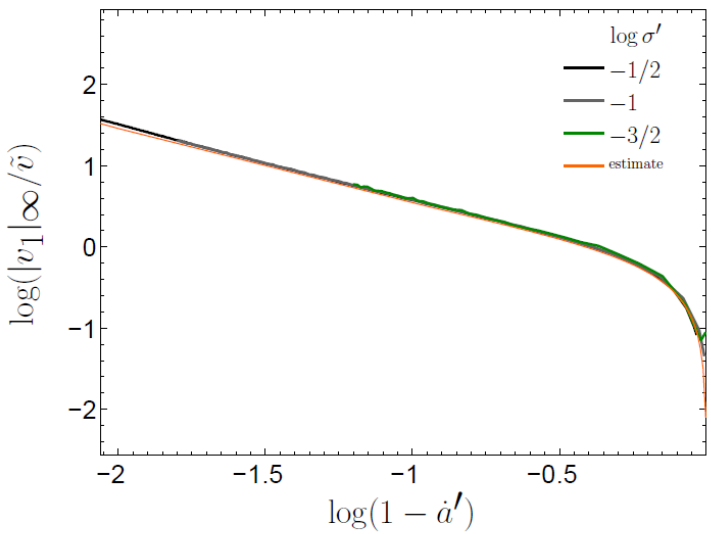

Low-amplitude loading, $\sigma' \ll 1$.

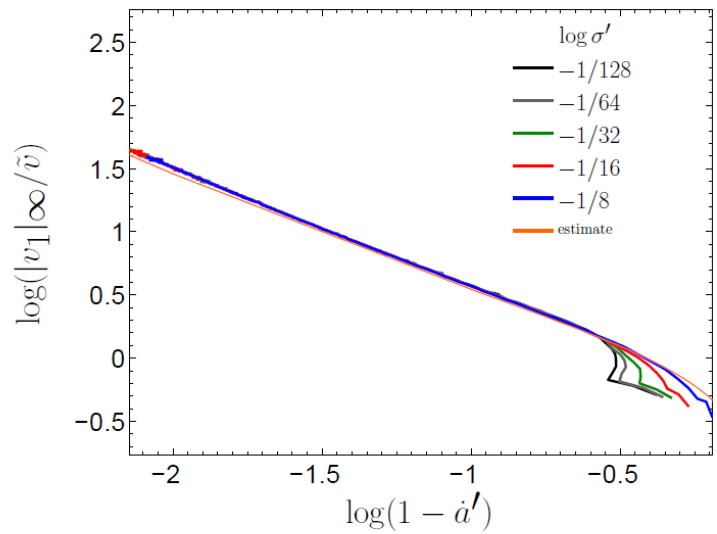

High-amplitude loading, $\sigma' \to 1^-$.

Relation to LEFM

$$\mathbf{s} = \frac{K\Sigma}{\sqrt{2\pi r}} + \text{higher order terms}$$

- LEFM solution is “acceptable” when Small Scale Yielding (SSY) holds:

SSY: The size of nonlinear fracture zone is very small compared to relevant length scales in the problem.

- Singular radius is the relevant length scale for dynamic case:

$r_{(k)}$ = size of region where singular term dominates for stress

- Fracture zone size: dynamic cohesive process zone is an estimate for “nonlinear fracture zone:

$$\Lambda_{(k)} = \zeta_{(k)}\pi \frac{\mu}{1-\nu} \frac{\tilde{\phi}_{(k)}}{(\tilde{\sigma}_{(k)})^2} \frac{1}{A_{(k)}(\hat{v})}$$

Linear Elastic Fracture Mechanics (LEFM)SSY indicator

$$\frac{\Lambda_{(k)}}{r_{(k)}} = \zeta_{(k)}\pi^2 \frac{\tilde{\phi}_{(k)}}{G}\left(\frac{\breve{\sigma}^k}{\tilde{\sigma}_{(k)}}\right)^2$$

- not strongly sensitive to crack velocity (as opposed to velocity field for quasi-singular response)
- $\sigma' = \frac{\bar{\sigma}}{\tilde{\sigma}} \propto \frac{\breve{\sigma}}{\tilde{\sigma}}$ is a nondimensional cohesive parameter.
- SSY indicator: General loading and geometry, dynamic loading

$$\lambda' = \zeta\pi^2\sigma'^2 \ll 1$$

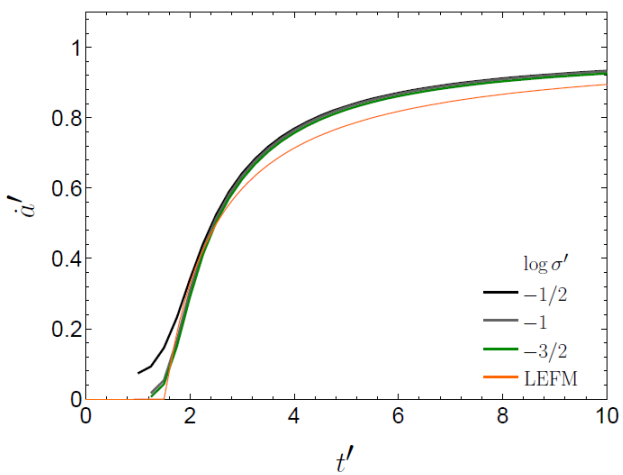

Low-amplitude loading, $\sigma' \ll 1$.

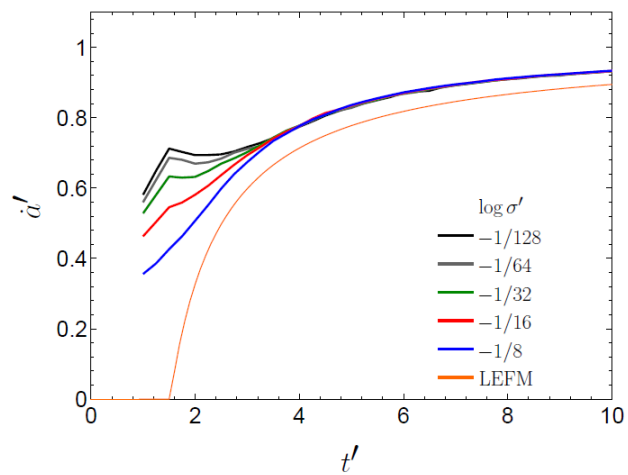

High-amplitude loading, $\sigma' \to 1^-$.

Traction Separation Laws Dimensional Analysis

- Intrinsic cohesive scales

$$\tilde{\phi} = \tilde{\sigma}\tilde{\delta} \qquad \text{Energy}$$

$$\tilde{p} = \rho\tilde{v} = \frac{\tilde{\sigma}}{c_{\mathrm{d}}} \qquad \text{Linear momentum}$$

$$\tilde{E} = \frac{\tilde{v}}{c_{\mathrm{d}}} = \frac{\tilde{\sigma}}{\rho c_{\mathrm{d}}^2} \propto \frac{\tilde{\sigma}}{\|\mathbf{C}\|} \qquad \text{Strain}$$

$$\tilde{v} = \frac{\tilde{\delta}}{\tilde{\tau}} = \frac{\tilde{\sigma}}{\rho c_{\mathrm{d}}} \qquad \text{Velocity}$$

$$\tilde{L} = c_{\mathrm{d}}\tilde{\tau} = \frac{\rho c_{\mathrm{d}}^2 \tilde{\delta}}{\tilde{\sigma}} \propto \Lambda^0 \qquad \text{Length}$$

$$\tilde{\tau} = \frac{\rho c_{\mathrm{d}} \tilde{\delta}}{\tilde{\sigma}} \qquad \text{Time}$$

$\tilde{\tau}$ is used for:

- Crack initiation and propagation
- Minimum numerical time step

- Nondimensional parameters
  - Spacetime: $L/\tilde{L}$ and $T/\tilde{\tau}$
  - Applied loads:

$$\bar{u}/\tilde{\delta}$$

$$\bar{v}/\tilde{v},\ c_{\mathrm{d}}\bar{E}/\tilde{v}$$

$$\bar{p}/\tilde{p},\ \bar{\sigma}/\tilde{\sigma}$$

$$\tilde{\tau}\bar{b}/\tilde{v}$$

- $L/\tilde{L}$ Determines brittleness; related to brittleness indicators of Carpinteri (03), Harder (91)
- $\frac{\tilde{\sigma}}{\|\mathbf{C}\|}$ is not a nondimensional parameter (it is often used as a nondimensional cohesive strength)

Part II:
Dynamically consistent solutions for contact modes

Integrated Fracture/Contact model
Mesoscopic interface subdivisions

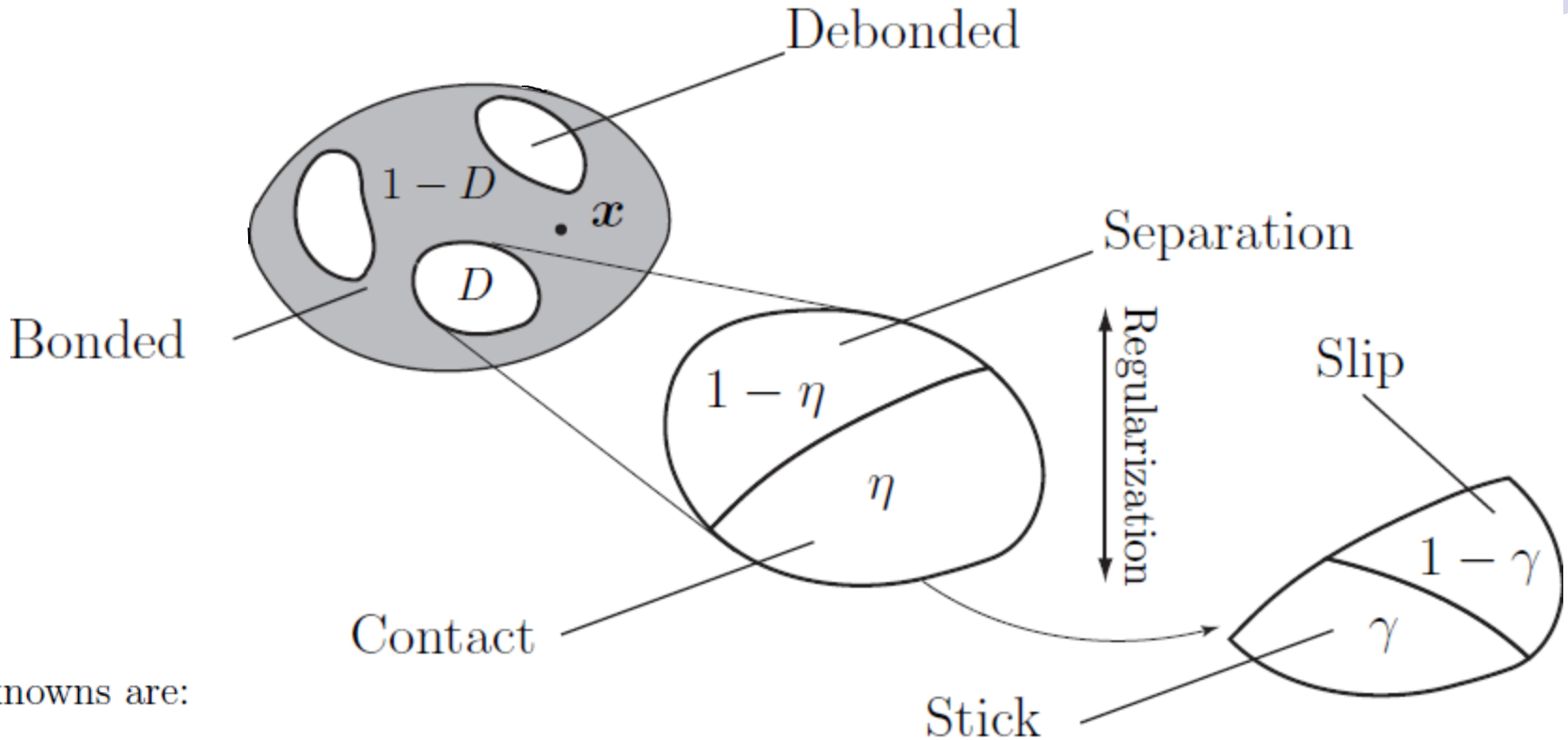

Unknowns are:

1. Target fluxes on individual subdivisions
2. Absolute area fractions of subdivisions:
   - Bonded & contact–stick (I) : $(1-D)+D\eta\gamma$
   - Contact–slip (II) : $D\eta(1-\gamma)$
   - Separation (III) : $D(1-\eta)$

- $D=1$ for pure contact problems; obtained from a fracture evolution law otherwise.
- Relative contact (η) and stick (γ) area fractions discussed on pages 4 & 5.

Riemann problem set-up

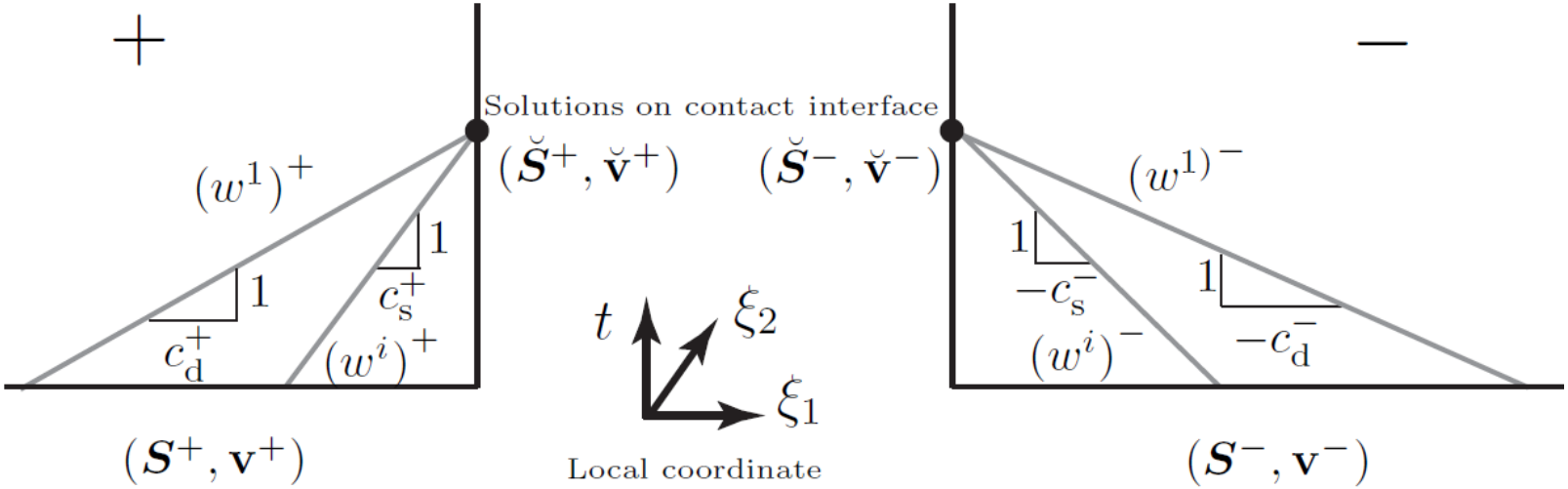

- $\boldsymbol{S}$: stress, $\boldsymbol{v}$: velocity
- c_{d}, c_{s}:

dilatational and shear wave speeds

- $w^{i\pm}$: characteristic values =

$s^{i\pm} \mp Z^{i\pm} v_{\underline{i}}^{\pm}$

- $Z^{i\pm}$: Impedance values =

$$\begin{cases} \rho^{\pm} c_{\mathrm{d}}^{\pm} & i = 1 \\ \rho^{\pm} c_{\mathrm{s}}^{\pm} & i \neq 1 \end{cases}$$

- $\boldsymbol{s} = S\mathbf{e}$: traction
- ρ: material density

Known:

upstream (interior traces): $\boldsymbol{S}^{\pm}, \boldsymbol{v}^{\pm}$

Goal:

Riemann solutions on contact interface : $\breve{\boldsymbol{S}}^{\pm}, \breve{\boldsymbol{v}}^{\pm}$

Property:

$w^{i\pm}$ preserved along characteristic directions

Riemann solutions

contact mode	interface conditions	Riemann solutions
bonded & contact–stick	$\breve{\boldsymbol{s}}^+ = \breve{\boldsymbol{s}}^- := \breve{\boldsymbol{s}}$ $\breve{\boldsymbol{v}}^+ = \breve{\boldsymbol{v}}^- := \breve{\boldsymbol{v}}$	$\breve{s}^i = \dfrac{w^{i+}Z^{i-} + w^{i-}Z^{i+}}{Z^{i-}+Z^{i+}}$ $= \dfrac{s^{i+}Z^{i-} + s^{i-}Z^{i+}}{Z^{i-}+Z^{i+}} + \dfrac{Z^{i-}Z^{i+}}{Z^{i-}+Z^{i+}}[\![v_i]\!]$ $\breve{v}_i = \dfrac{[\![w^i]\!]}{Z^{i-}+Z^{i+}} = \dfrac{[\![s^i]\!]}{Z^{i-}+Z^{i+}} + \dfrac{v_i{}^+Z^{i+} + v_i{}^-Z^{i-}}{Z^{i-}+Z^{i+}}$
contact–slip	$\breve{s}^{1+} = \breve{s}^{1-} := \breve{s}^1$ $\breve{v}_1^+ = \breve{v}_1^- := \breve{v}_1$ $\breve{\boldsymbol{\tau}}^+ = \breve{\boldsymbol{\tau}}^- := \breve{\boldsymbol{\tau}} = k\langle -\breve{s}^1\rangle_+ \mathbf{e}_{\breve{\mathbf{v}}}$	$\breve{s}^1, \breve{v}_1 =$ same as contact–stick solution $\breve{s}^i = k\langle -\breve{s}^1\rangle_+ \mathbf{e}^i_{\breve{\boldsymbol{\tau}}}$ $\breve{v}_i^\pm = \pm\dfrac{\breve{s}^i - w^{i\pm}}{Z^{i\pm}} = v_i^\pm + \dfrac{\breve{s}^i - s^{i\pm}}{Z^{i\pm}}$
separation	$\breve{\boldsymbol{s}}^+ = \breve{\boldsymbol{s}}^- := \breve{\boldsymbol{s}} = \mathbf{0}$	$\breve{\boldsymbol{s}} = \mathbf{0}$ $\breve{v}_i^\pm = \mp\dfrac{w^{i\pm}}{Z^{i\pm}} = v_i^\pm - \dfrac{s^{i\pm}}{Z^{i\pm}}$

$\breve{\boldsymbol{\tau}} := \breve{s}^2\mathbf{e}_2 + \breve{s}^3\mathbf{e}_3$: tangential traction at contact interface

$\mathbf{e}_{\breve{\mathbf{v}}}$: unit vector along the velocity jump from contact–slip solution

$\mathbf{e}_{\breve{\boldsymbol{\tau}}}$: unit vector along the tangential traction from contact–stick solution

Contact Transitions: Contact-Separation (C-S)

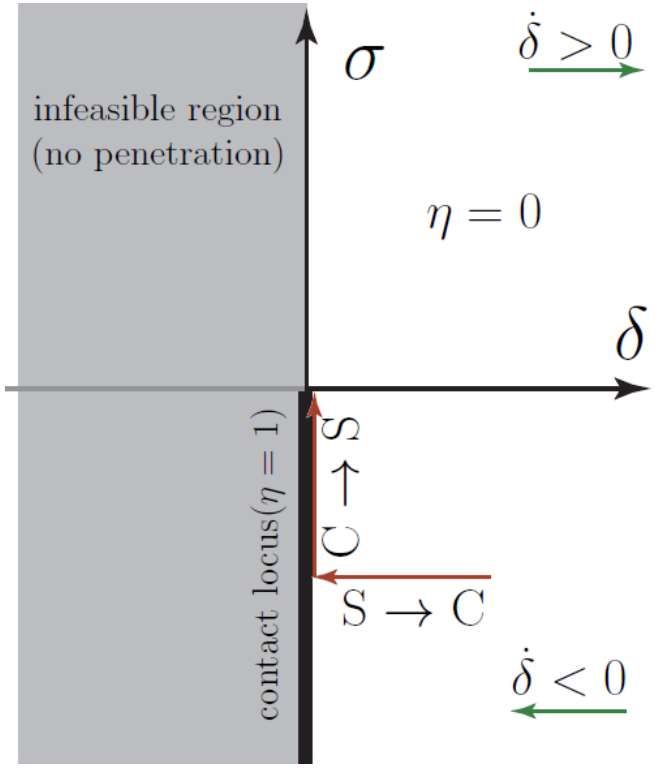

Provable Max. Penetration

No stiff systems

σ: normal contact–stick Riemann traction

δ: normal separation

Sharp transition

Regularized

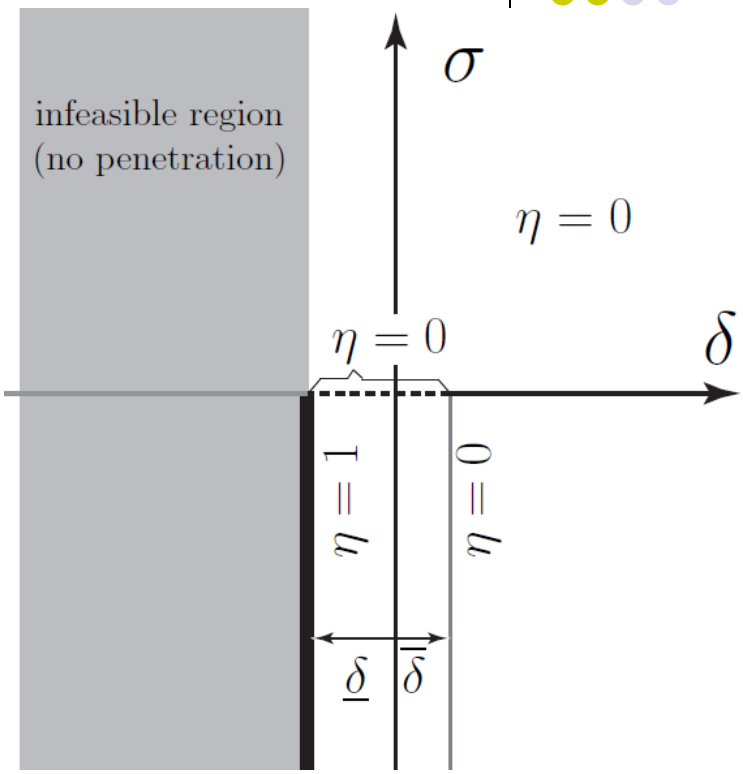

Only S $\rightarrow$ C:

- occurs at constant σ $\Rightarrow$
- introduces shocks $\Rightarrow$
- requires regularization

t', δ': normalized time and penetration

$\eta = g(t') \;\Rightarrow \delta' = h(t') \;\Rightarrow \eta = f(\delta')$, where $f = g \circ h^{-1}$

- $g(t')$: ideal to design well-behaved & C^1 regularization
- $f(\delta')$: computationally favorable; δ' readily available
- Example for regularization design ($g \;\rightarrow\; f$):

$$g(t') = 1 - \cos(\tfrac{\pi}{2}t') \quad \Rightarrow \quad f(\delta') = 1 - \sqrt{1 - \delta'^2}$$

Contact Transitions: Stick-Slip

Coulomb friction law:

- In slip mode: tangential traction ($\check{\boldsymbol{\tau}}$) is aligned with velocity jump ($[\![\check{\boldsymbol{v}}]\!]$):

  $\check{\boldsymbol{\tau}} = k\langle -\check{s}^1\rangle_+ \mathbf{e}_{\check{\mathbf{v}}}$

  But $[\![\check{\boldsymbol{v}}]\!] = 0$ at the transition $\Rightarrow$

  - $\mathbf{e}_{\check{\mathbf{v}}}$ is not defined at the transition
  - Transition is <u>apparently</u> discontinuous
    - Many "numerical treatments" are presented to address the problem

---

Riemann solutions for Coulomb friction law $\Rightarrow$

$[\![\check{\boldsymbol{v}}]\!] = \frac{Z^{2+}+Z^{2-}}{Z^{2+}Z^{2-}}\left(|\check{\boldsymbol{\tau}}| - |\check{\boldsymbol{\tau}}|\right)\mathbf{e}_{\check{\boldsymbol{\tau}}} \Rightarrow \quad (\check{\boldsymbol{\tau}}:$ contact–stick tangential stress$)$

- $\mathbf{e}_{\check{\mathbf{v}}} = \mathbf{e}_{\check{\boldsymbol{\tau}}}$
- At the transition $|\check{\boldsymbol{\tau}}| = k\langle -\check{s}^1\rangle_+ > 0 \Rightarrow |\check{\boldsymbol{\tau}}| > 0$. That is:
  - $\mathbf{e}_{\check{\boldsymbol{\tau}}}$ is <u>continuous</u> at the transition
  - The representation $\check{\boldsymbol{\tau}} = k\langle -\check{s}^1\rangle_+ \mathbf{e}_{\check{\boldsymbol{\tau}}}$:
    - <u>Eliminates the need for regularization</u>
    - γ only takes the binary values of 0 and 1

Numerical verification: Identical bars

Benchmark problem [Hughes (76);Laursen, Chawla (97); Czekanski, Meguid (01); Cirak, West (05); *etc.*]

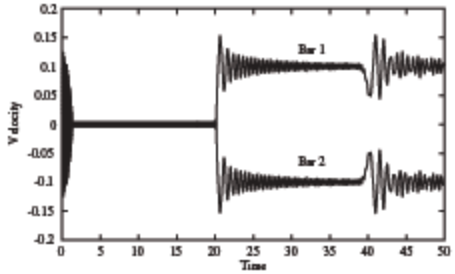

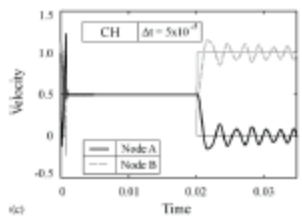

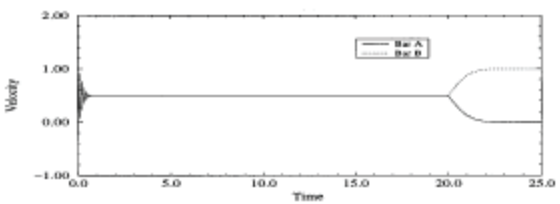

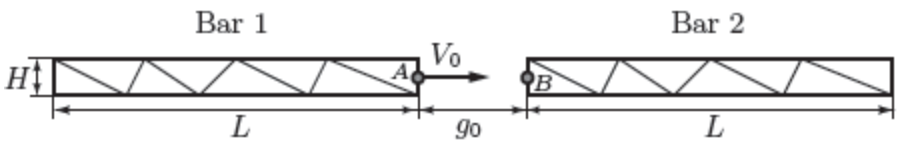

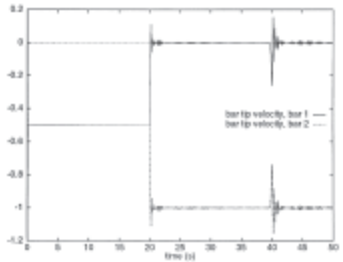

Riemann solutions incorporated in *Spacetime Discontinuous Galerkin* finite element method

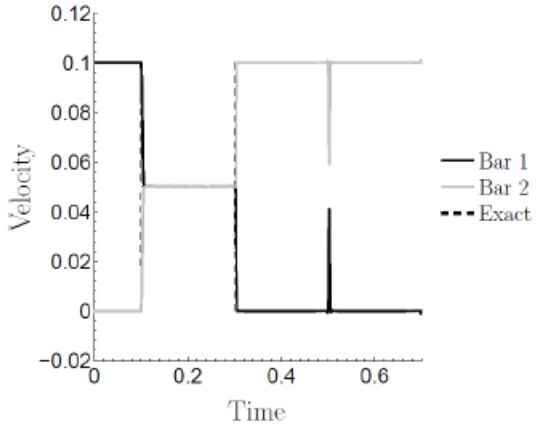

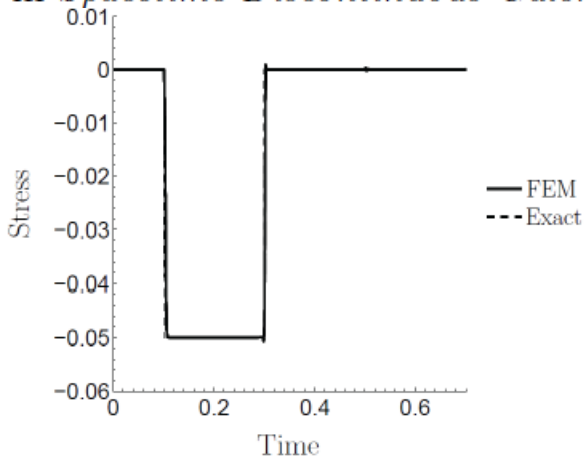

Unlike other solutions, SDG results are not overly damped and are free of numerical oscillations and overshoot / undershoot

Contact Transitions: Stick-Slip

Coulomb friction law:

- In slip mode: tangential traction ($\check{\boldsymbol{\tau}}$) is aligned with velocity jump ($[\![\check{\boldsymbol{v}}]\!]$):

  $\check{\boldsymbol{\tau}} = k\langle -\check{s}^1\rangle_+ \mathbf{e}_{\check{\mathbf{v}}}$

  But $[\![\check{\boldsymbol{v}}]\!] = 0$ at the transition $\Rightarrow$

  - $\mathbf{e}_{\check{\mathbf{v}}}$ is not defined at the transition
  - Transition is <u>apparently</u> discontinuous
    - Many "numerical treatments" are presented to address the problem

---

Riemann solutions for Coulomb friction law $\Rightarrow$

$[\![\check{\boldsymbol{v}}]\!] = \frac{Z^{2+}+Z^{2-}}{Z^{2+}Z^{2-}}\left(|\check{\boldsymbol{\tau}}| - |\check{\boldsymbol{\tau}}|\right)\mathbf{e}_{\check{\boldsymbol{\tau}}} \Rightarrow \quad (\check{\boldsymbol{\tau}}:$ contact–stick tangential stress$)$

- $\mathbf{e}_{\check{\mathbf{v}}} = \mathbf{e}_{\check{\boldsymbol{\tau}}}$
- At the transition $|\check{\boldsymbol{\tau}}| = k\langle -\check{s}^1\rangle_+ > 0 \Rightarrow |\check{\boldsymbol{\tau}}| > 0$. That is:
  - $\mathbf{e}_{\check{\boldsymbol{\tau}}}$ is <u>continuous</u> at the transition
  - The representation $\check{\boldsymbol{\tau}} = k\langle -\check{s}^1\rangle_+ \mathbf{e}_{\check{\boldsymbol{\tau}}}$:
    - <u>Eliminates the need for regularization</u>
    - γ only takes the binary values of 0 and 1

Brake simulation
Contact mode transitions (high slip velocity)

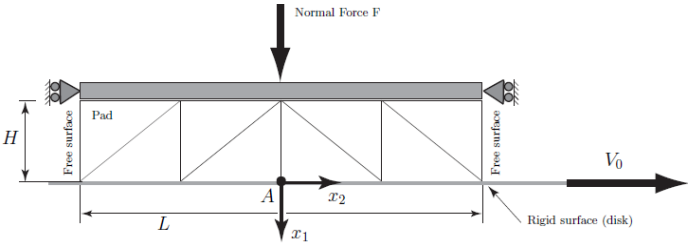

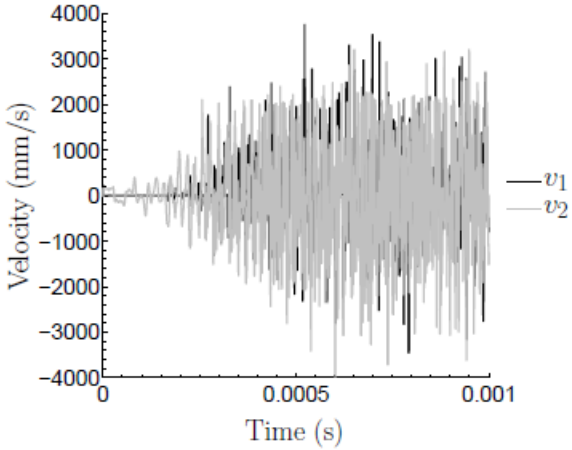

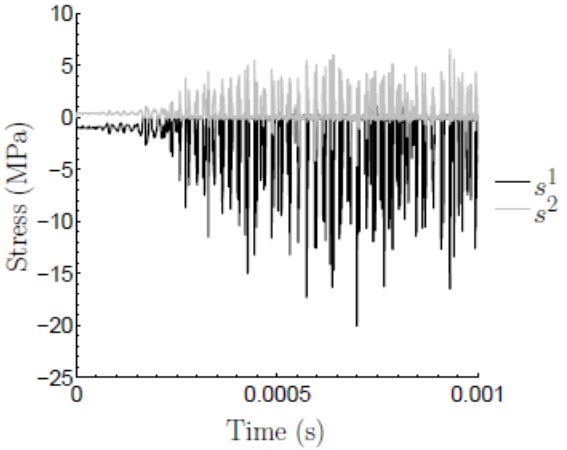

Depending on sliding velocity there are different mode transitions:

V_0:

Low	:	stick-slip
Medium	:	stick-slip-separation
High	:	slip-separation

Histories presented at point A

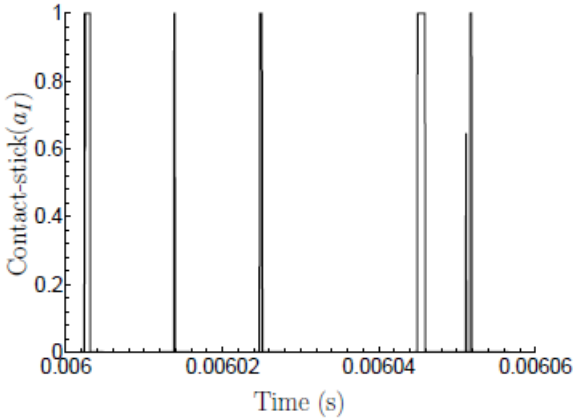

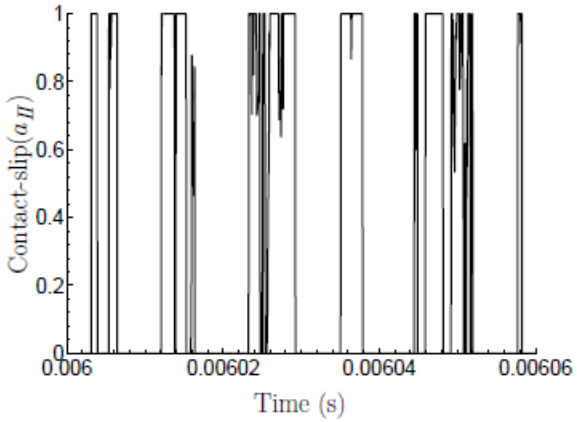

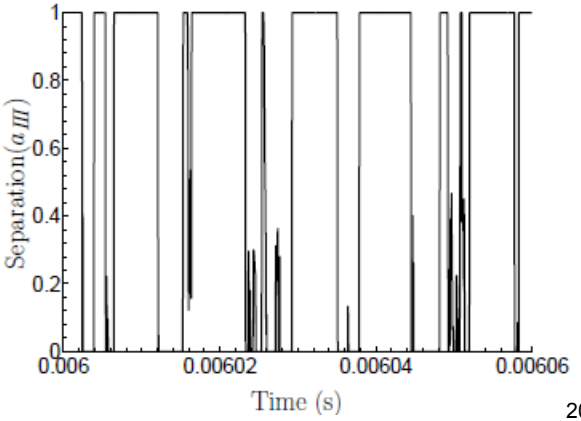

Brake simulation
Contact mode transitions (high slip velocity)

click to play movie

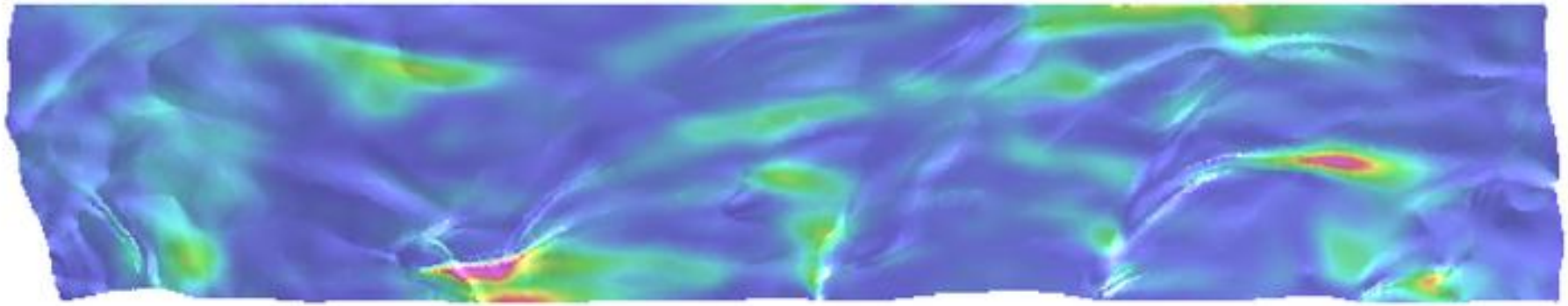

Color: strain energy; Height: velocity

Key points of the contact model

- Opposed to contact models that prevent node penetration at discrete level, the formulation is continuum-based
- Solutions are for dynamic setting
- Riemann solutions preserve the characteristics of the elastodynamics problem
- Only separation to contact requires regularization
  - There is a maximum tunable penetration
  - The regularization is rather uniform and can be C^1 continuous
  - It does not make the problem stiff (unlike penalty methods for example)
- Numerical results do not exhibit nonphysical oscillations, excessive dissipation, overshoot, and undershoot
- Fracture (damage evolution) is easily incorporated

Part III:

An interfacial rate-dependent contact/fracture model

Interfacial rate-dependent damage model

Motivated by mesoscale features:

Conical (parabolic) marking on the crack surface

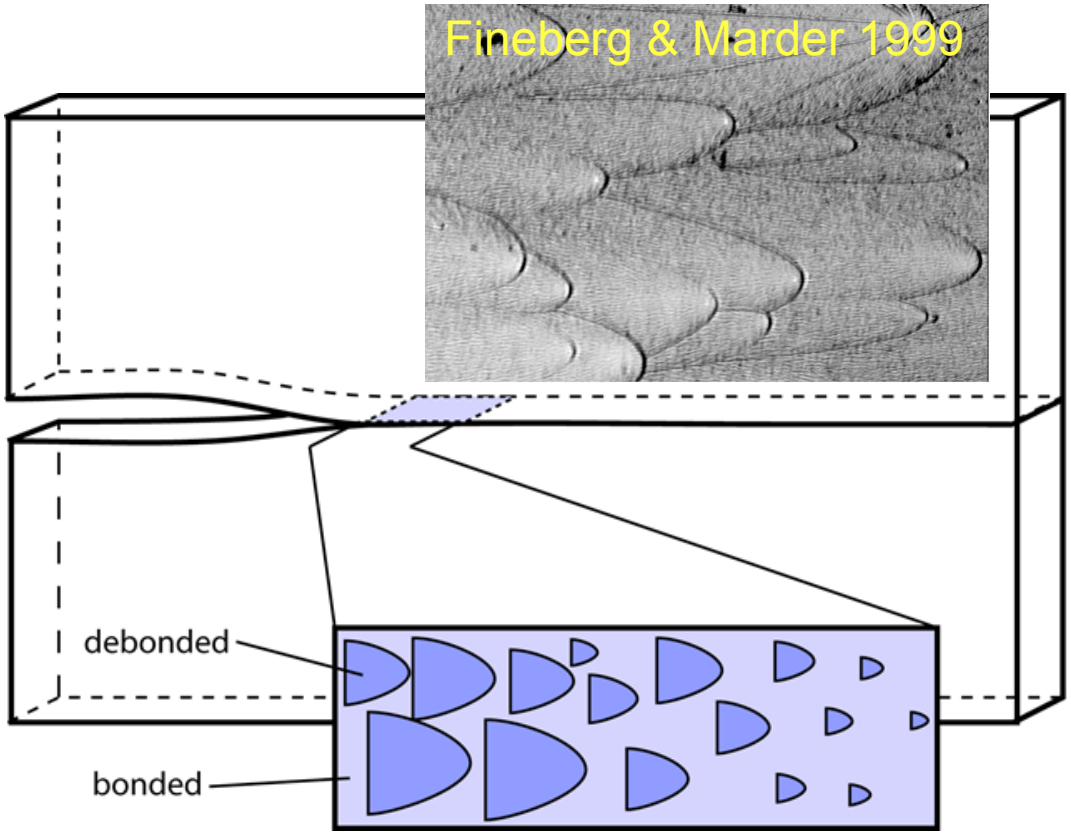

Ravi-Chandar, Knauss 1984

Damage evolution law

$$\dot{D} = \begin{cases} \frac{1}{\tilde{\tau}}[1 - H(\langle f(y) - D\rangle_+)] & D < 1 \\ 0 & D = 1 \end{cases} \qquad H(x) = \exp(-a.x)$$

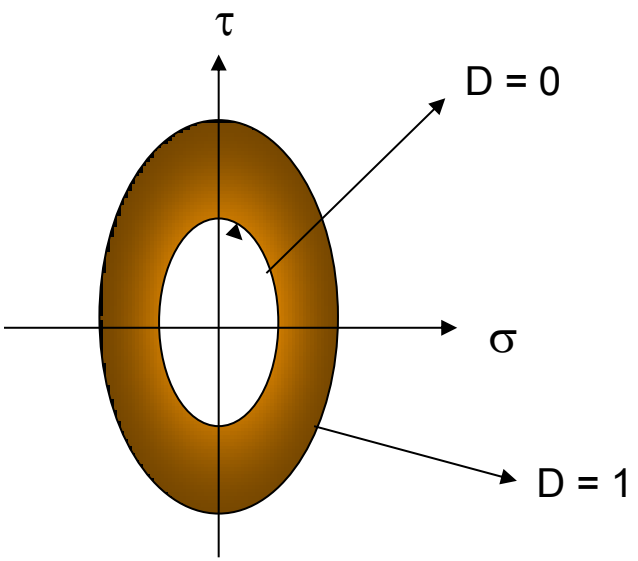

Properties of the evolution law

- a maximum damage rate, exists.
- Target damage value, $f(y)$, is a function of stress.
- The rate is a function of the difference between damage and its target value.

Key points of the damage model

- Based on a characteristic length $\tilde{\sigma}$ and characteristic time $\tilde{\tau}$.
- Damage is stress induced (Ravi-Chandar, Yang 1997).
- Rate-dependent damage model:
  - Hardening effects at high-strain rates (Fineberg & Marder 1999)
  - There is a maximum damage rate $\tilde{\tau}$.
  - Introduces a length (displacement) scale.
  - Eliminated the mesh dependency of static damage models (strain softening behavior, Bazant & Belytschko 1984)
- No artificial bulk compliance: Perfectly bonded initial response with no effect on bulk material response.
- Differentiable response (facilitates numerics).
- Dynamically consistent fluxes.
- Integrated contact modes.

Deeper understanding of fracture models
Comparison of cohesive and damage models

$$\tilde{\tau} = \frac{\tilde{\delta}\rho c_{\mathrm{d}}}{\tilde{\sigma}}$$

$$\tilde{\delta} = \frac{\tilde{\tau}\tilde{\sigma}}{\rho c_{\mathrm{d}}}$$

CFM

D

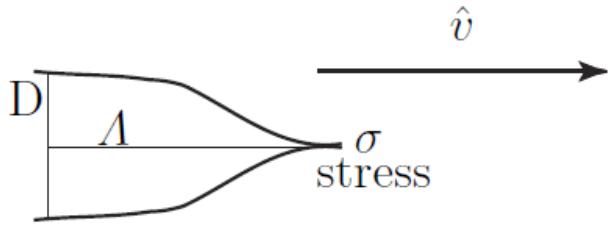

time for complete separation

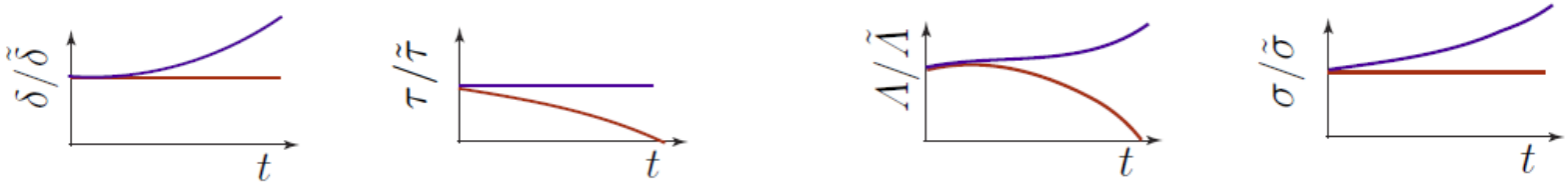

- While cohesive and interfacial damage models have the intrinsic scales, they behave very differently even when same nondimensional parameters are used.
- They have fundamentally different crack acceleration pattern ⇨

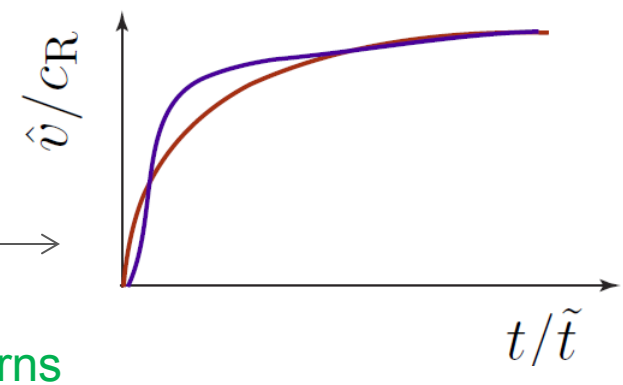

Very different dynamic crack propagation patterns

Contact/damage examples
Crack closure: cyclic, dynamic loading

click to play movie

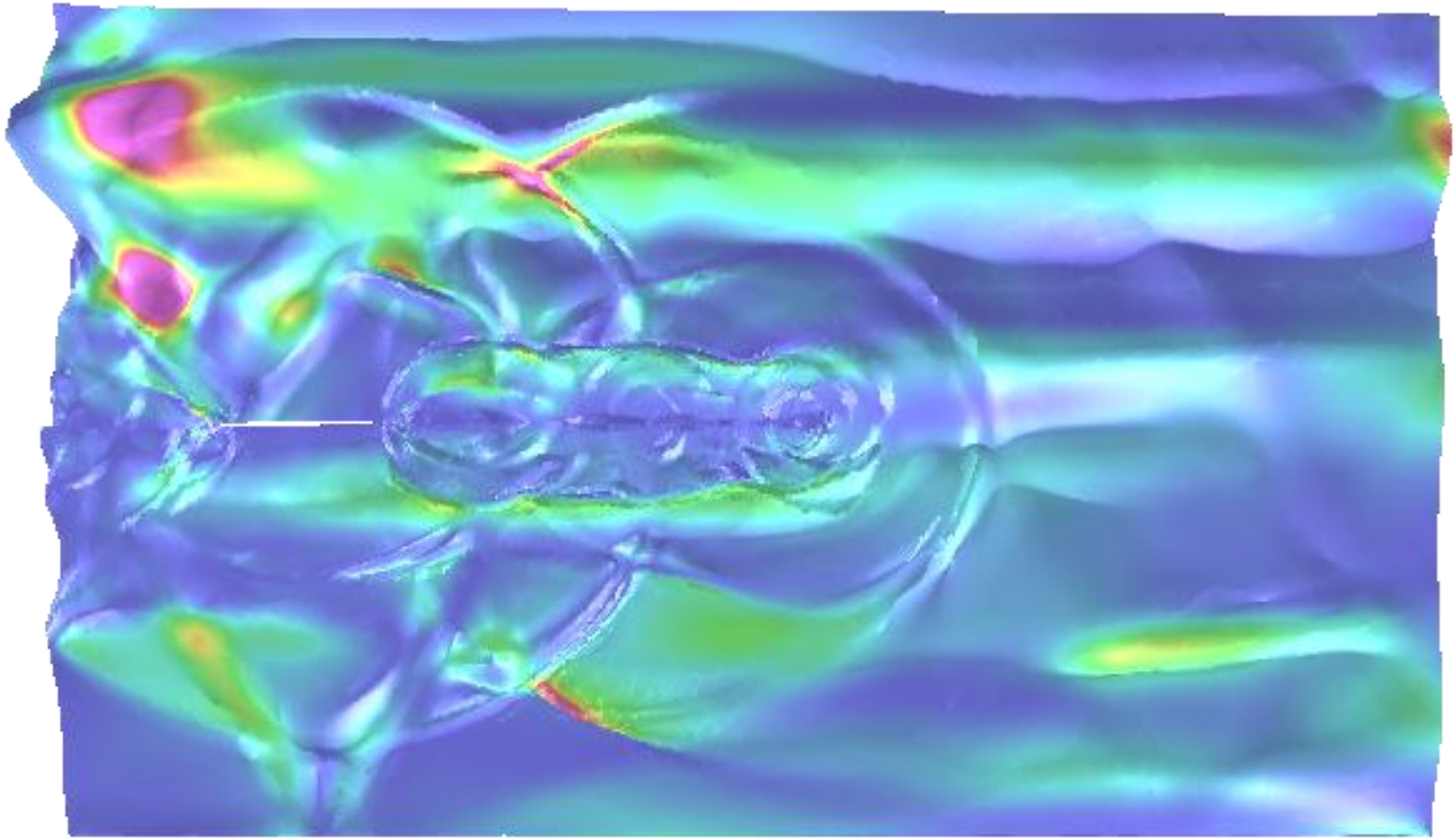

Color: log(strain energy); Height: velocity

Contact/damage examples
cyclic loading for a stiff circular inclusion

click to play movie

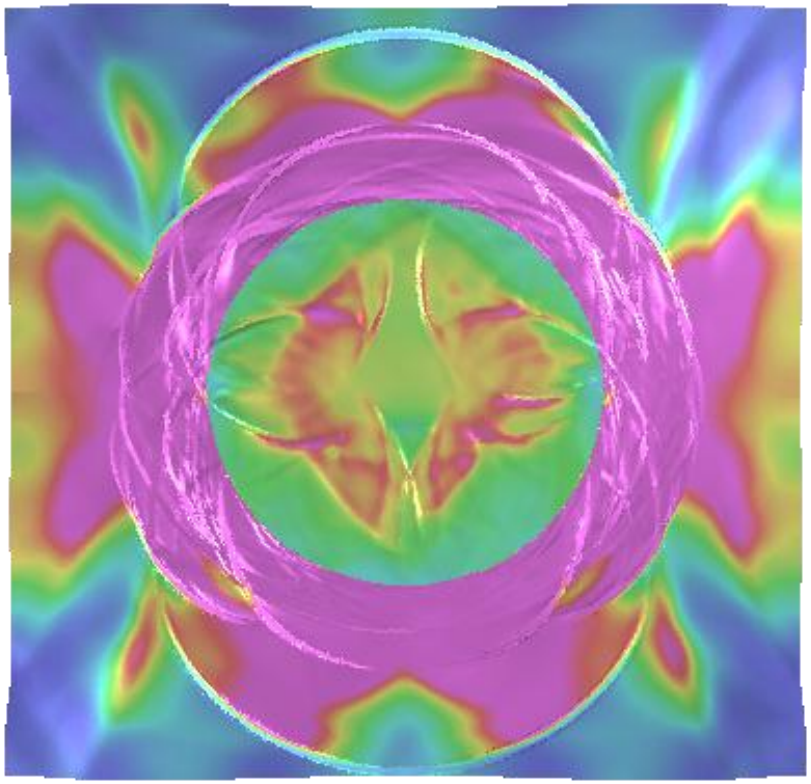

Color: log(strain energy);
Height: velocity

Part IV:
A probabilistic model for dynamic fracture

Solution-dependent crack path

Arbitrary crack extension:

- Element boundaries are aligned with arbitrary propagation direction by spacetime meshing operations.
- Unlike XFEM, no need to introduce discontinuous features within elements.
- Maximum effective stress governs direction.

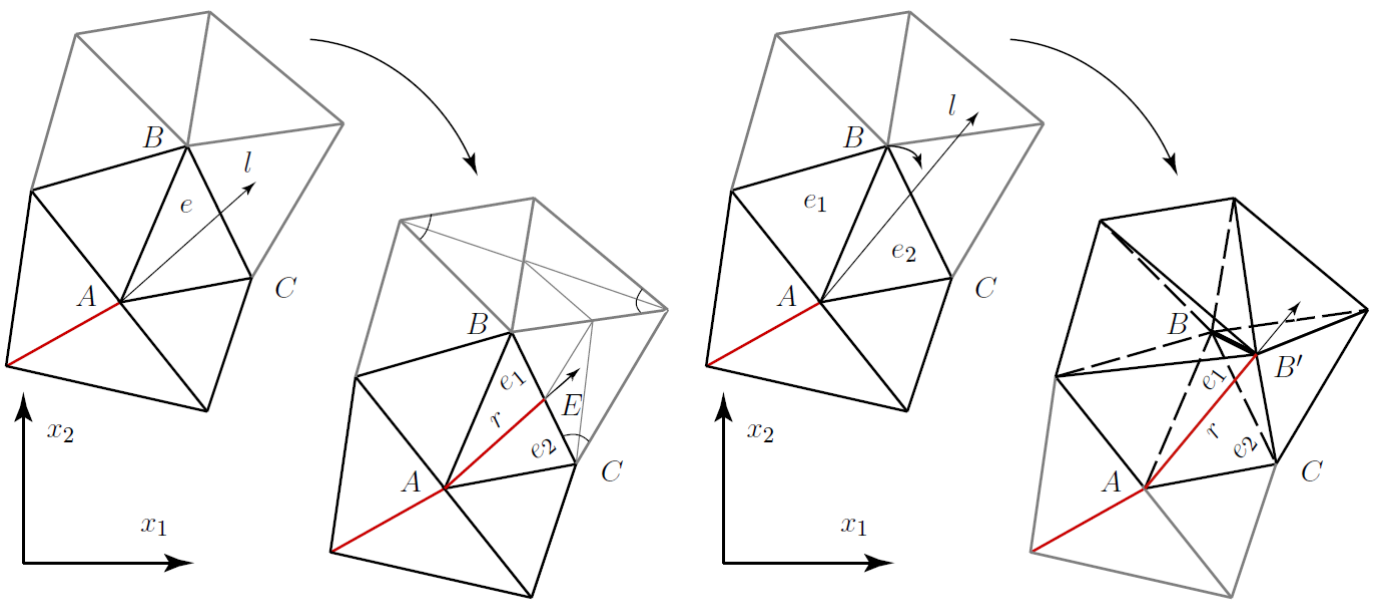

alignment by refinement operation

alignment in spacetime by tent pitching operation

Solution-dependent crack path

Probabilistic crack nucleation:

- Fracture process are inherently stochastic
- Deterministic & homogeneous treatments fail at continuum level!
- Cracks nucleate from defects with random distribution of strength

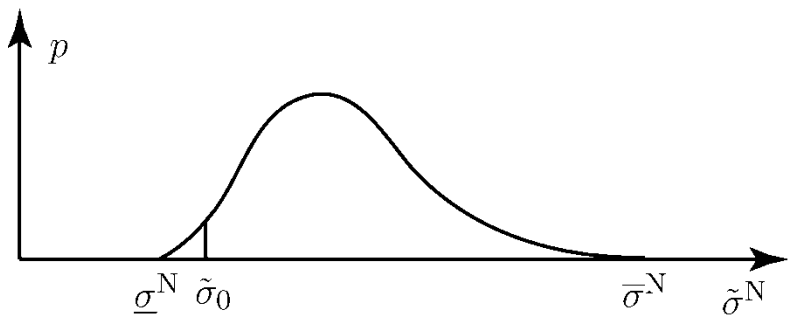

$n = \rho^{\mathrm{N}} a$

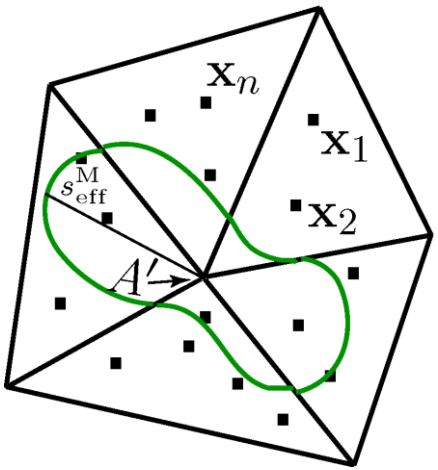

Instabilities: no additional criterion required to capture:

- Branching
- Microcracking
- Surface roughening

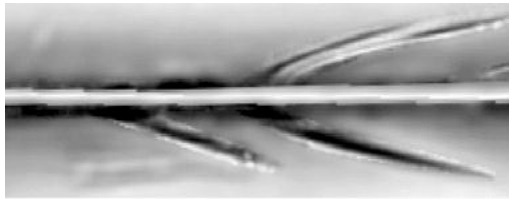

Dynamic fracture with damage-delay cohesive model, random defects and nucleation

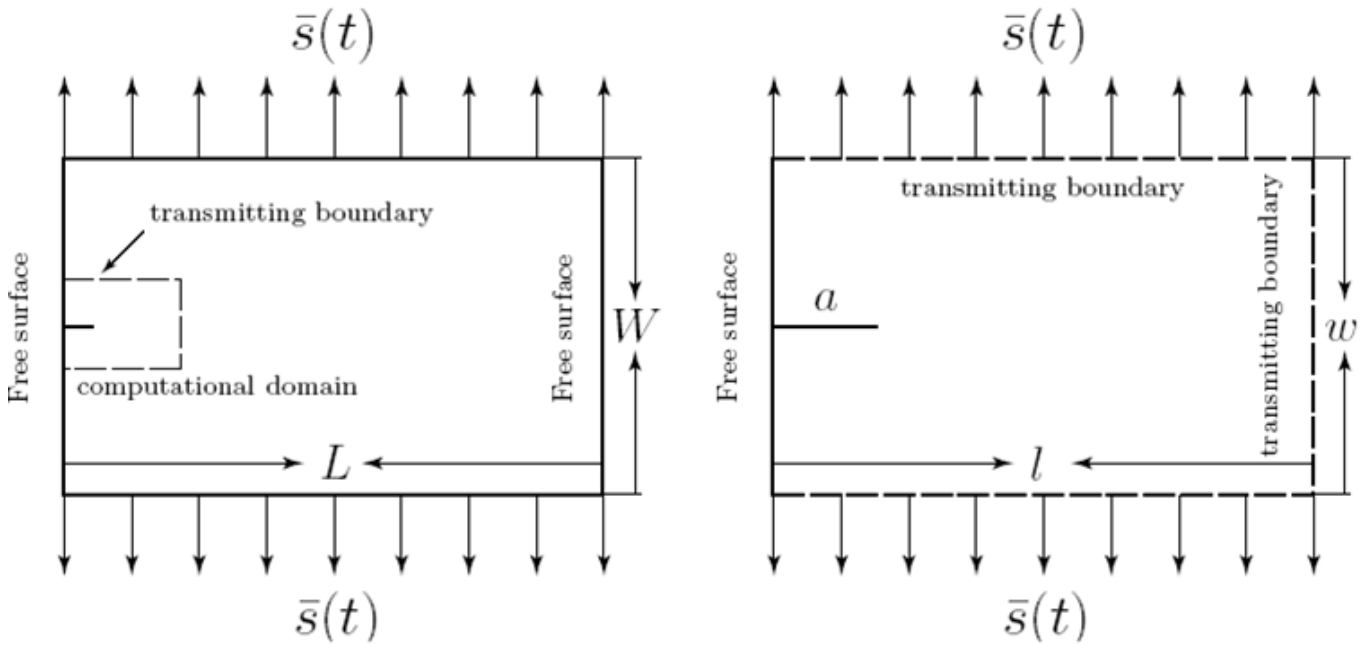

(a) The experimental setting. (b) The computational domain.

PMMA:

- $E = 3.24GPa.$
- $\rho = 1190\frac{Kg}{m^3}.$
- $w = 0.020MPa.$
- $\tau = 10^{-2}\mu s.$

based on Sharon and Fineberg experiment (1996)

Dynamic fracture
Spacetime mesh front

click to play movie

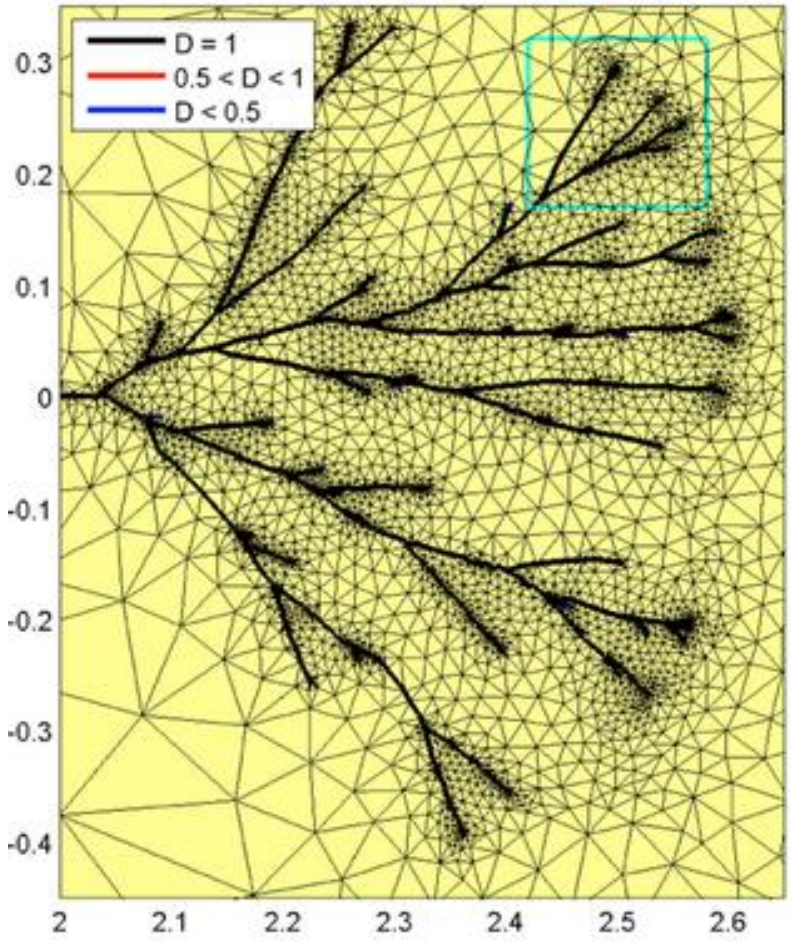

Dynamic fracture
Displaced shape

click to play movie

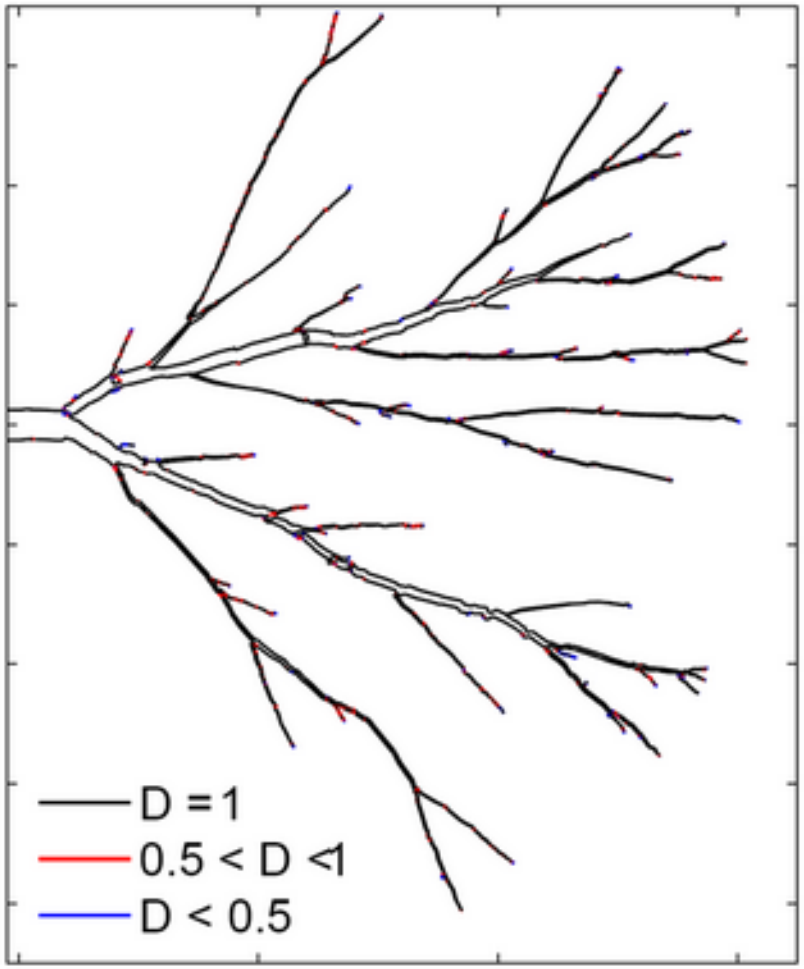

Refinement Details: 1 x zoom

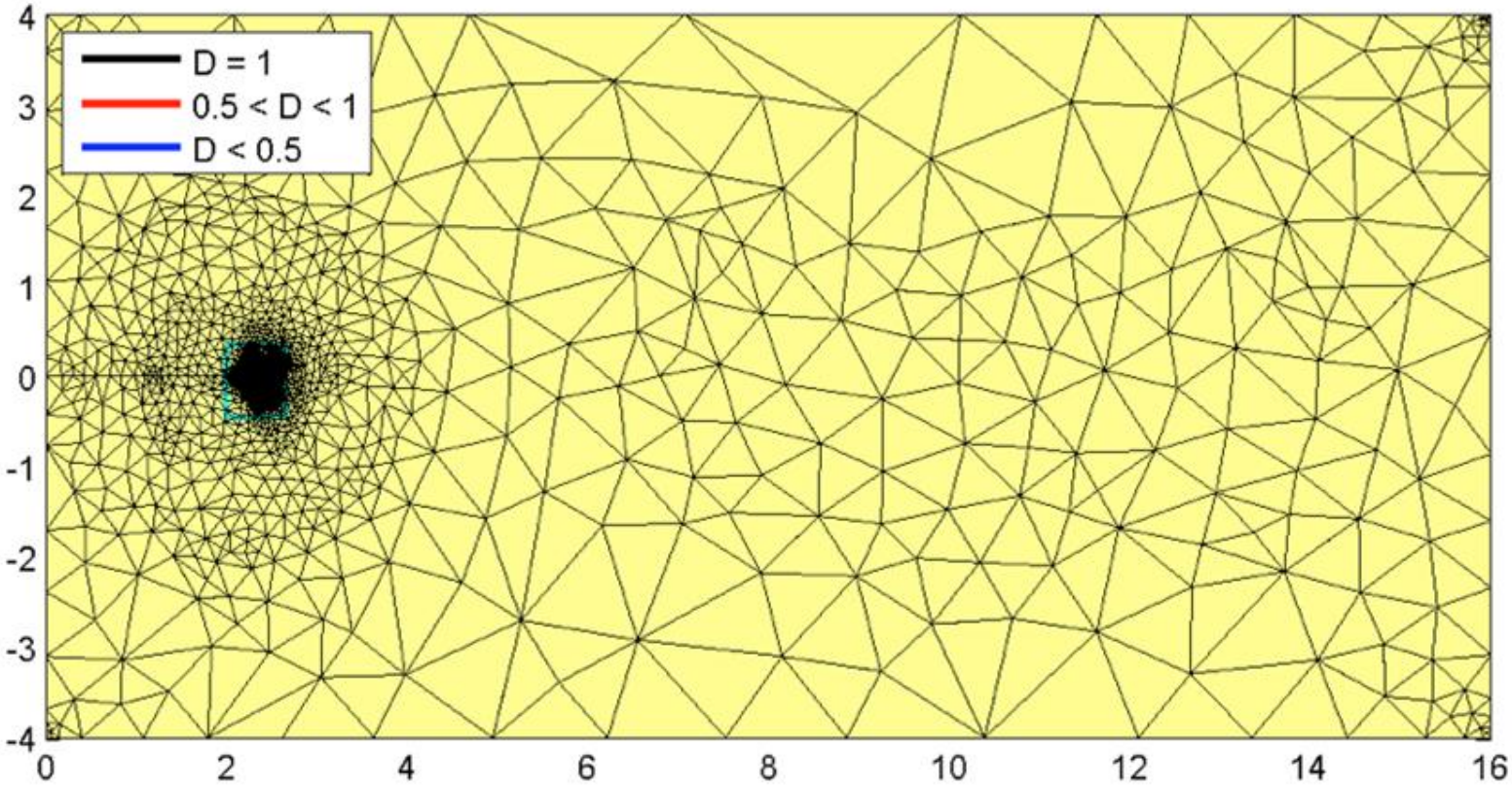

Refinement Details: 25 x zoom

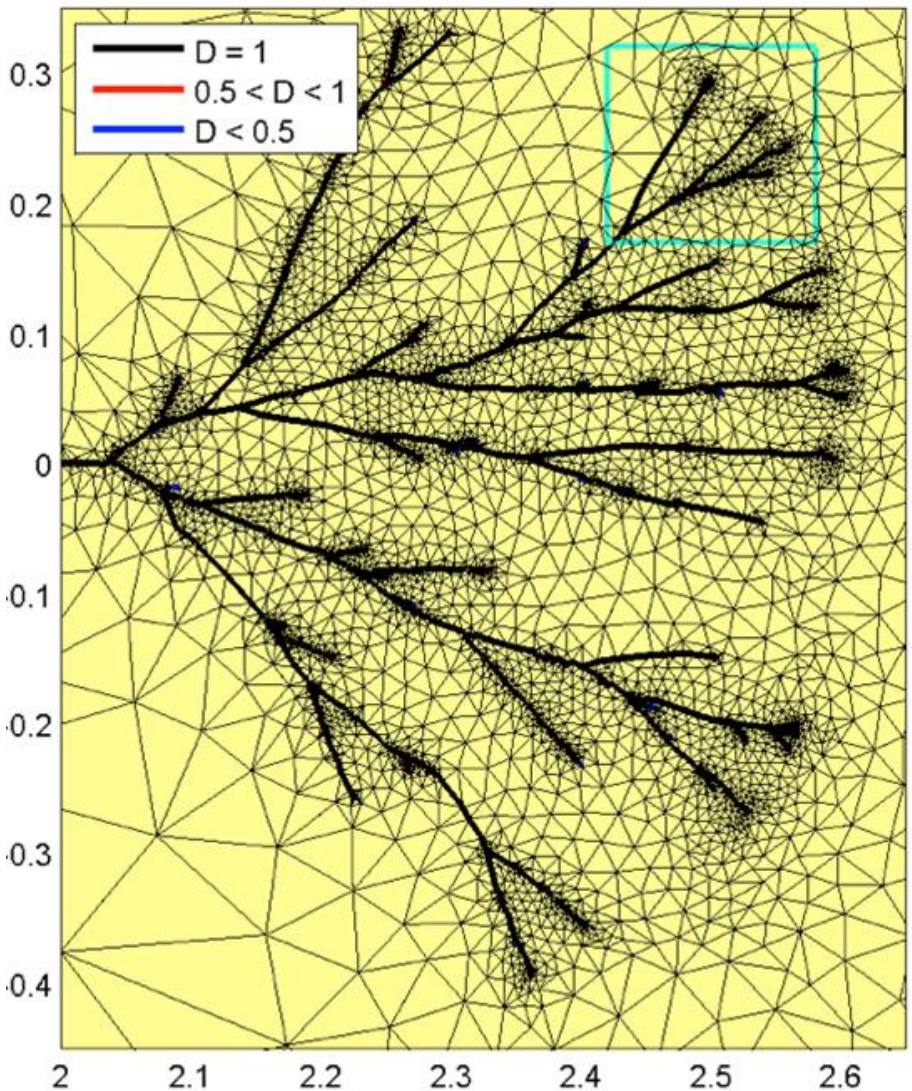

Crack-branching automatically follows from probabilistic nucleation model

Refinement Details: 100 x zoom

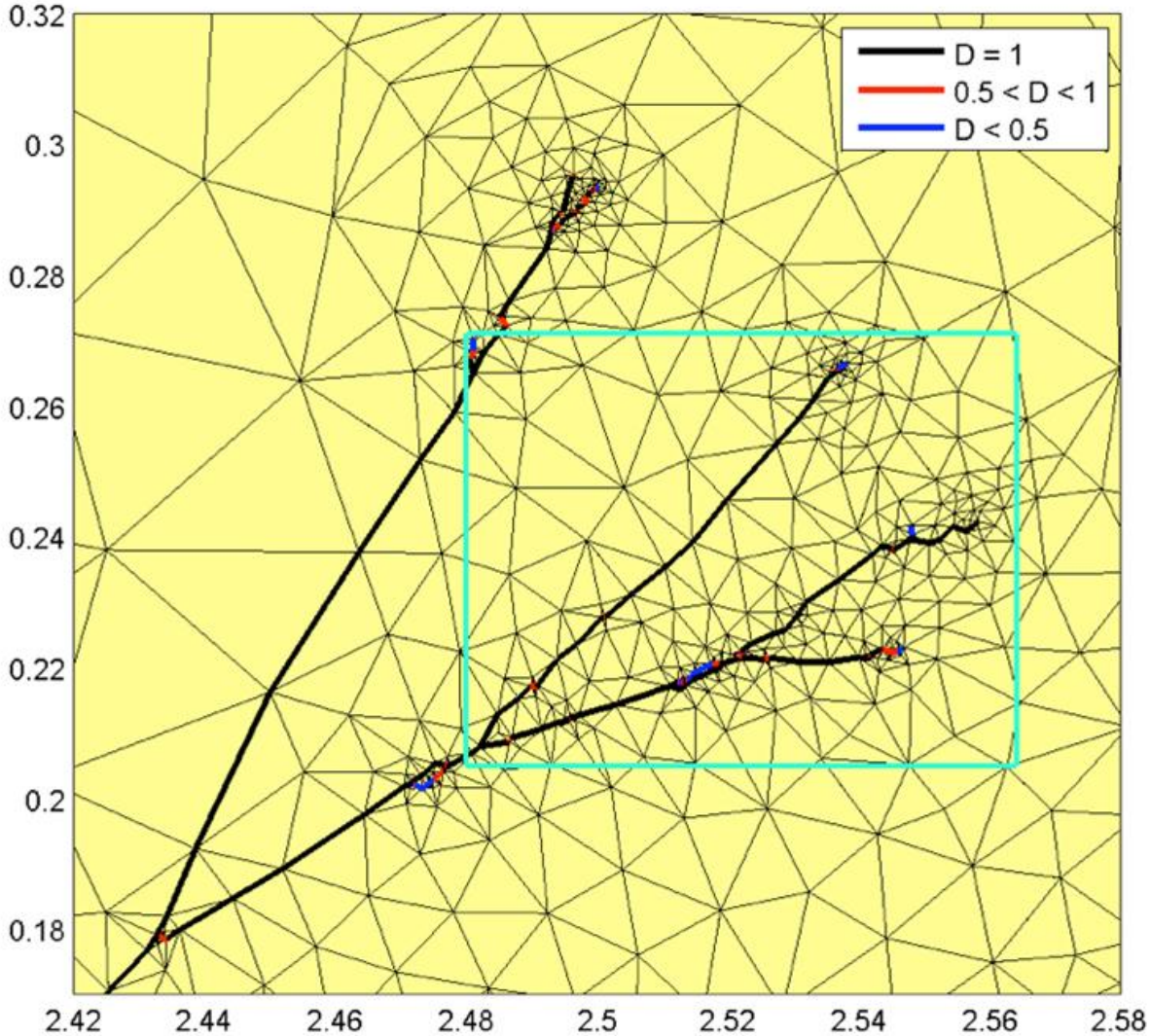

Refinement Details: 200 x zoom

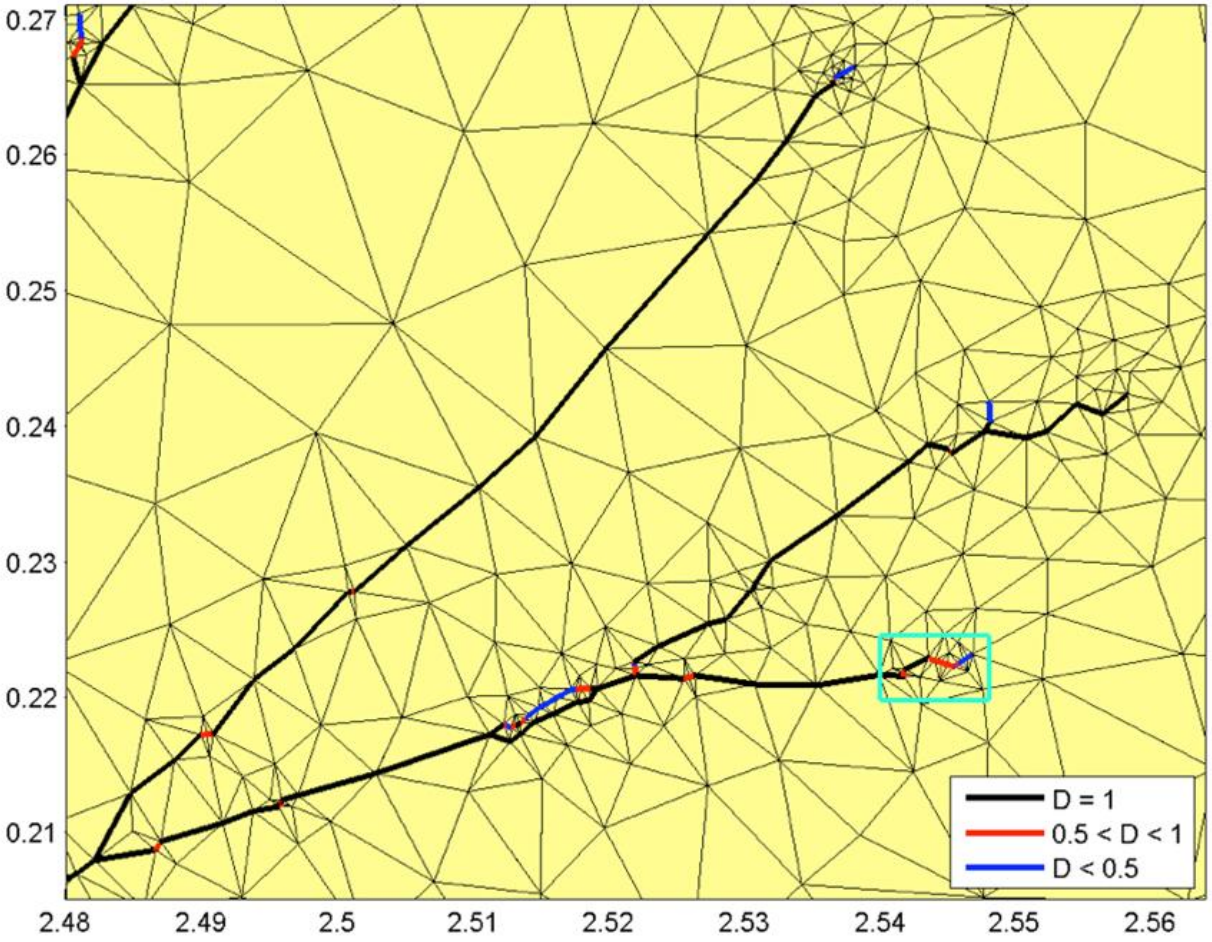

Crack path oscillation for higher crack speeds agrees with theoretical and experimental findings

Refinement Details: 2000 x zoom

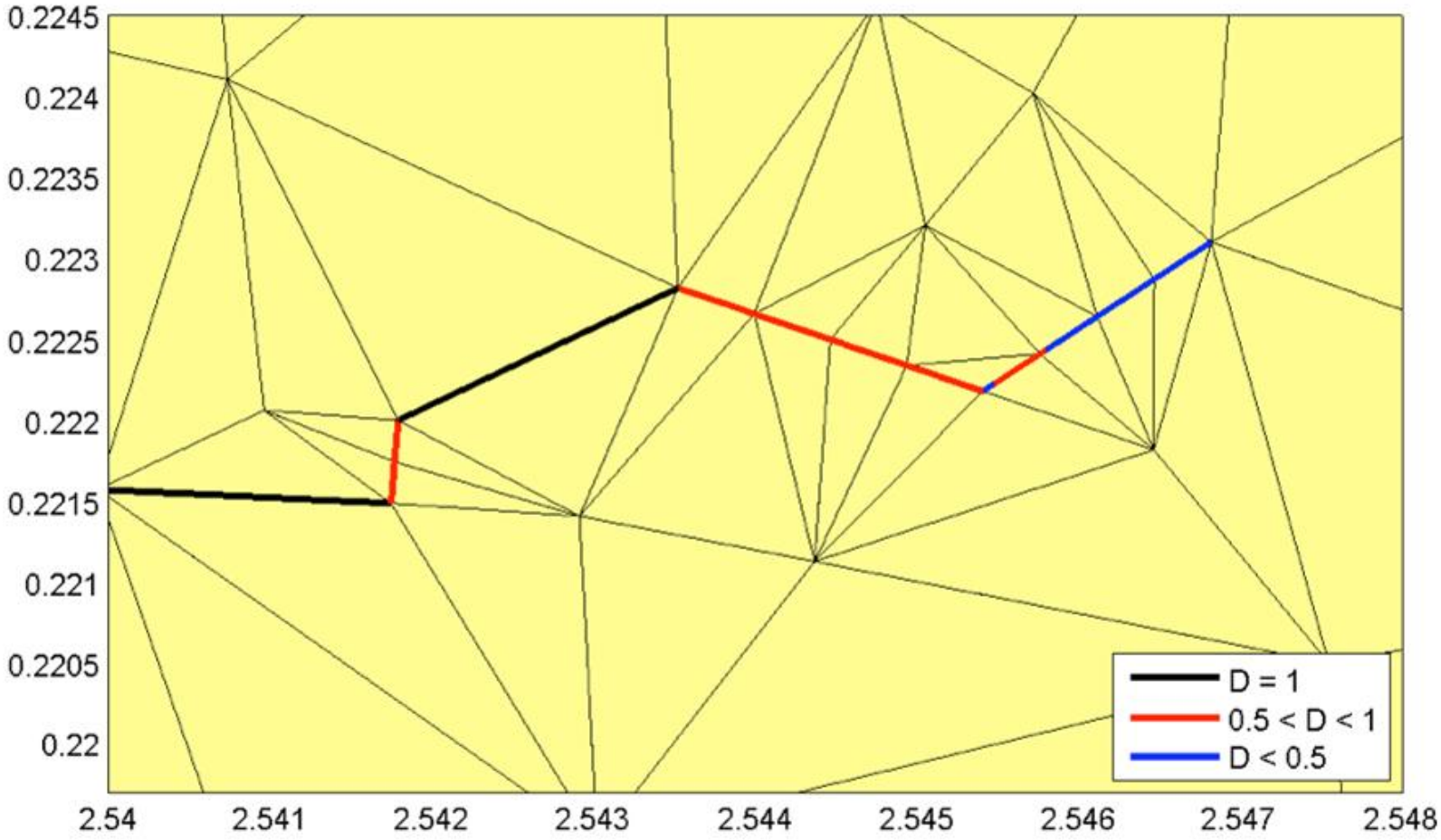

Part V:
Structural Health Monitoring for composite laminates
Forward analysis

Structural Health Monitoring in Layered Plate Systems

- Flaw detection and identification
  - Holes, through-cracks, delamination, bulk damage, etc.
  - Many layers with strong anisotropic response
- Detect and simulate changes in wave propagation
  - Precise physical excitation and sensing
  - Inverse problem to identify flaws (type, location, size, shape): requires many forward analyses

---

- Many forward analyses → efficiency
- to not only resolve the minute differences causes by defects, but also differentiate them from numerical artifacts → high accuracy and stability

⇒

SDG method is an ideal solver for SHM applications

Forward analysis
Plate with multiscale features (planar modes)

click to play movie

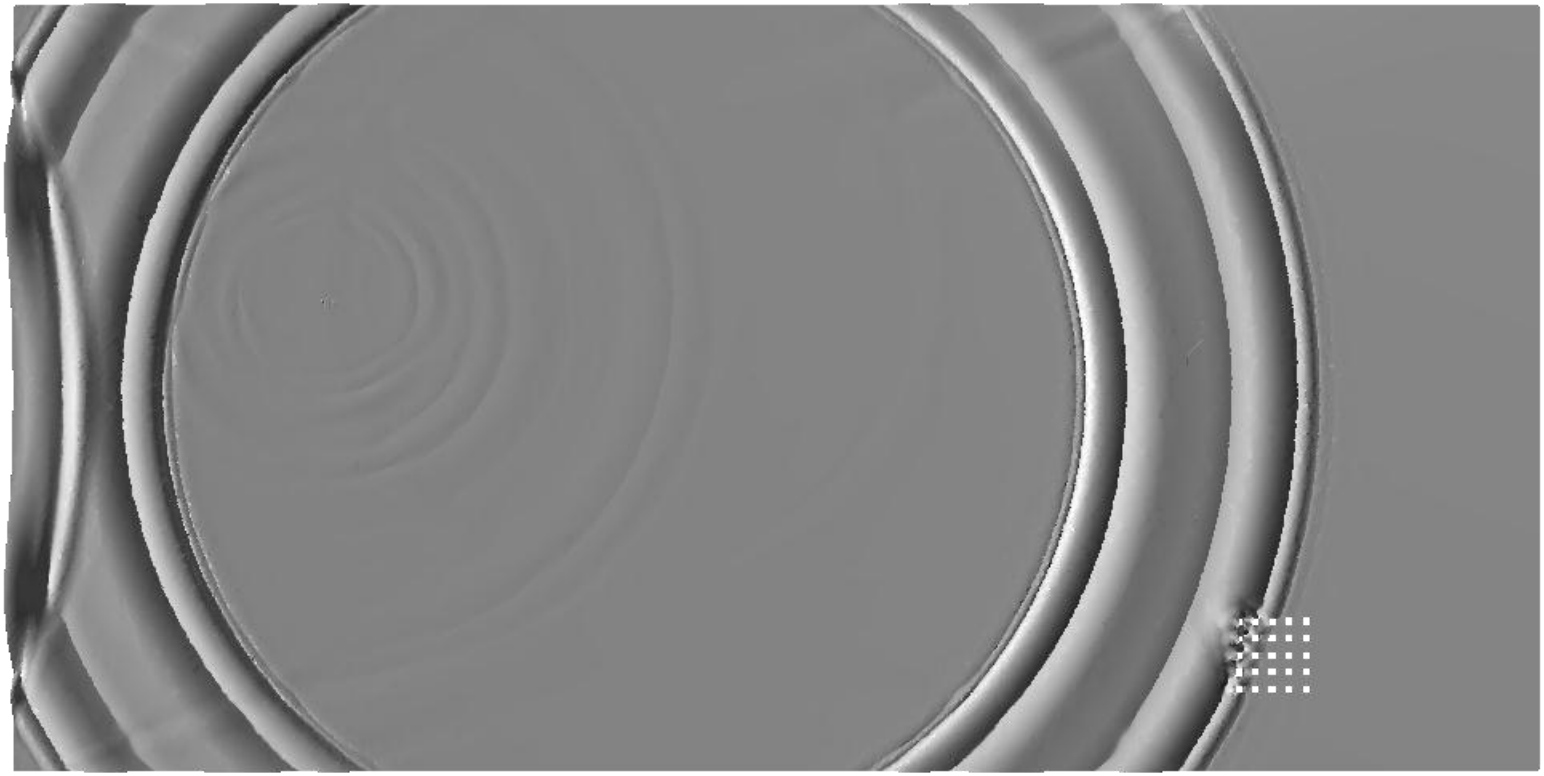

Height: velocity

Detection of arrays of defects from wave scattering:
Large defects at lower right corner & very small ones at upper left corner(cannot be seen)

Hybrid 2D/3D plate formulation

- Low order kinematic assumptions for thickness direction can introduce relative errors larger than 10 (e.g. multi-layer composite laminates).
- Difficulties in the derivation of 2D formulations for high order in-thickness kinematics.
- Full 3D analysis may be expensive and not suitable for specific thickness direction kinematic assumptions (e.g. zigzag interpolations)

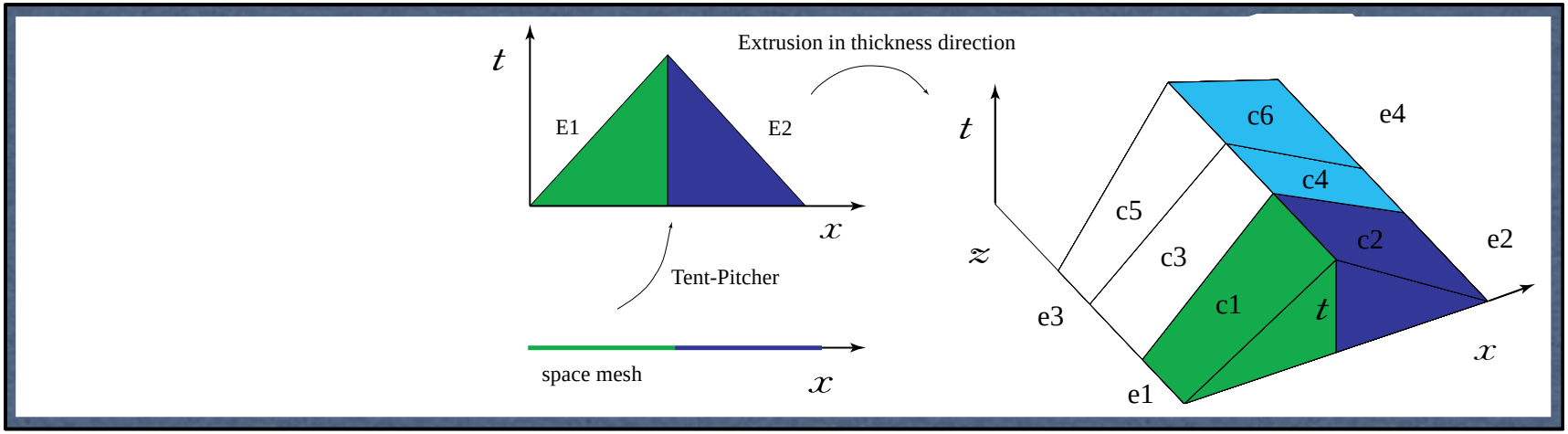

Application to multi-ply plates
(only front mesh shown below)

- Extrude 2D spatial geometry in transverse ‘thickness’ direction

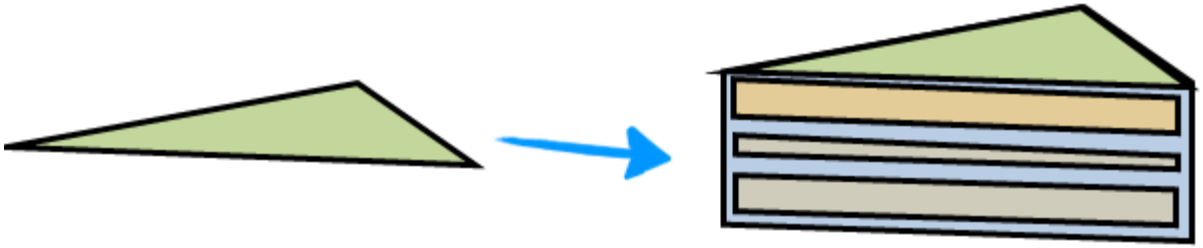

- Product bases: (in-plane) x (transverse) x (time)
  - Independent selections for (u,v) and (w) d.o.f.
  - Elements with multiple int. cells for simple layered plate model
    - First and higher-order shear-deformation-theory models
    - ‘Zig-zag’ layered plate model; C0 piecewise-linear basis
  - Multi-element model: one (element/int. cell) per layer
    - SDG models with per-ply dofs
    - Interface models for delamination
  - Higher-order and p-adaptive models
    - avoid shear correction factors; transitions to full 3D x time models

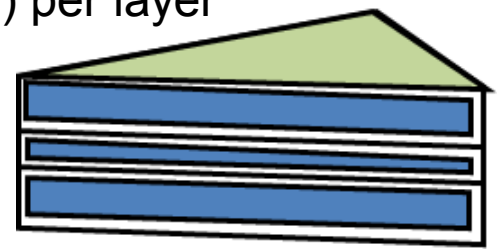

2-ply plate with flaw

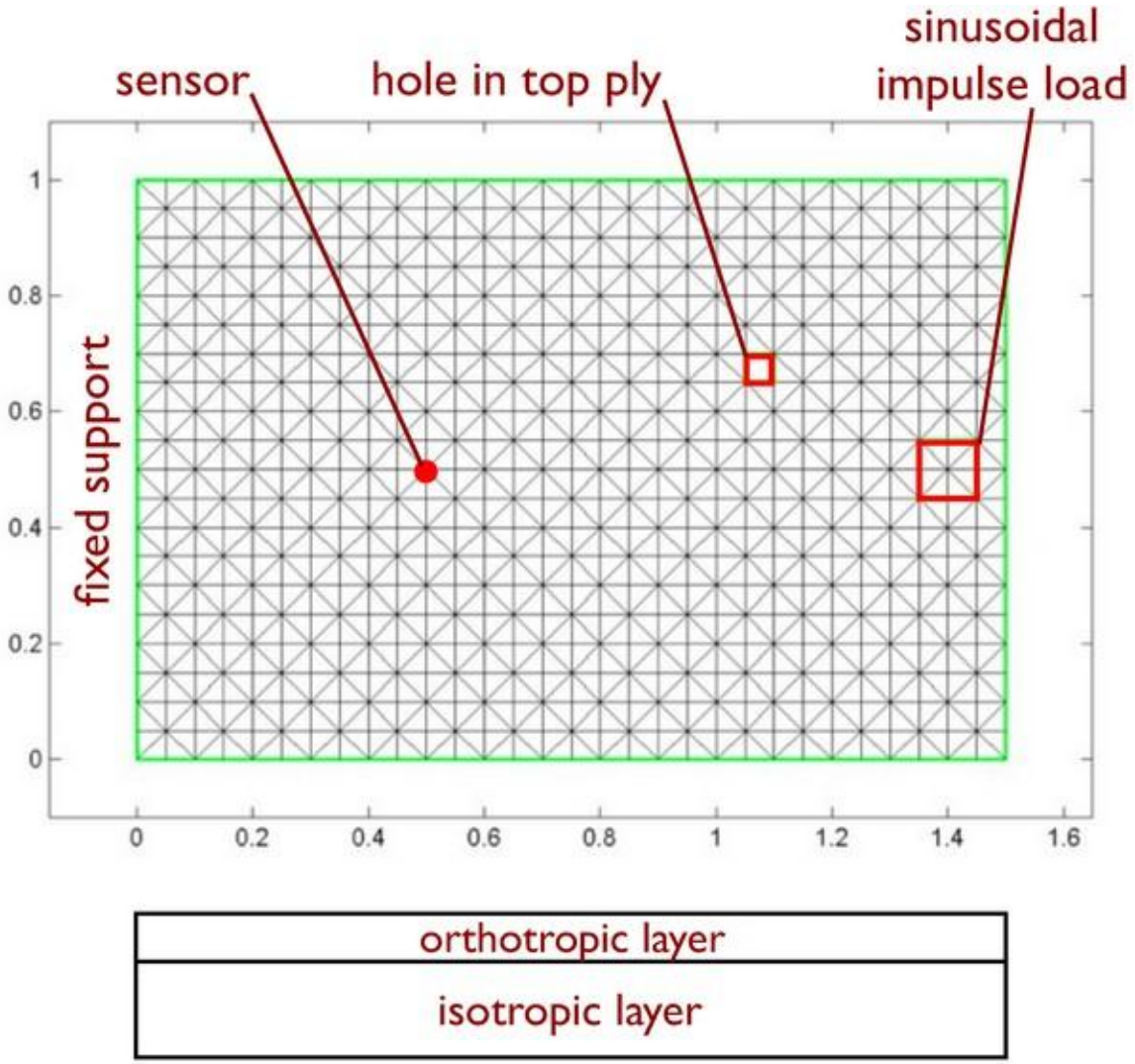

2-ply plate with flaw
Effect of flaw on velocity at sensor position

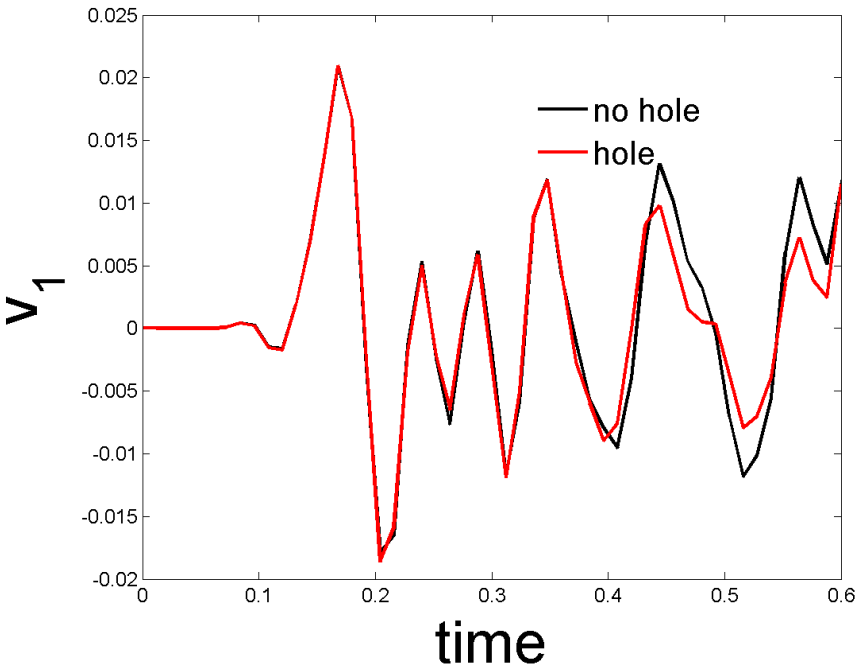

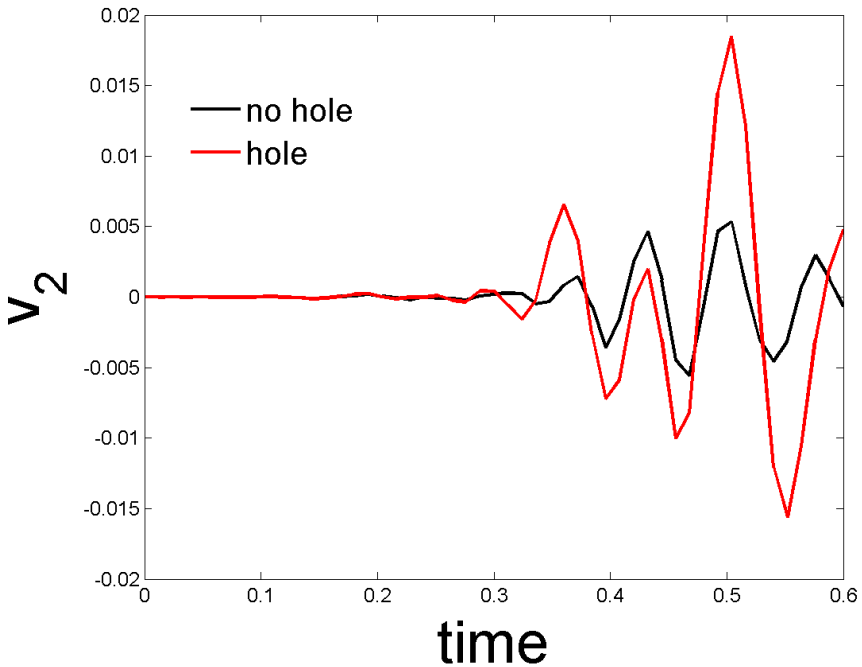

Forward analysis
Plate with multiscale features (planar modes)

click to play movie

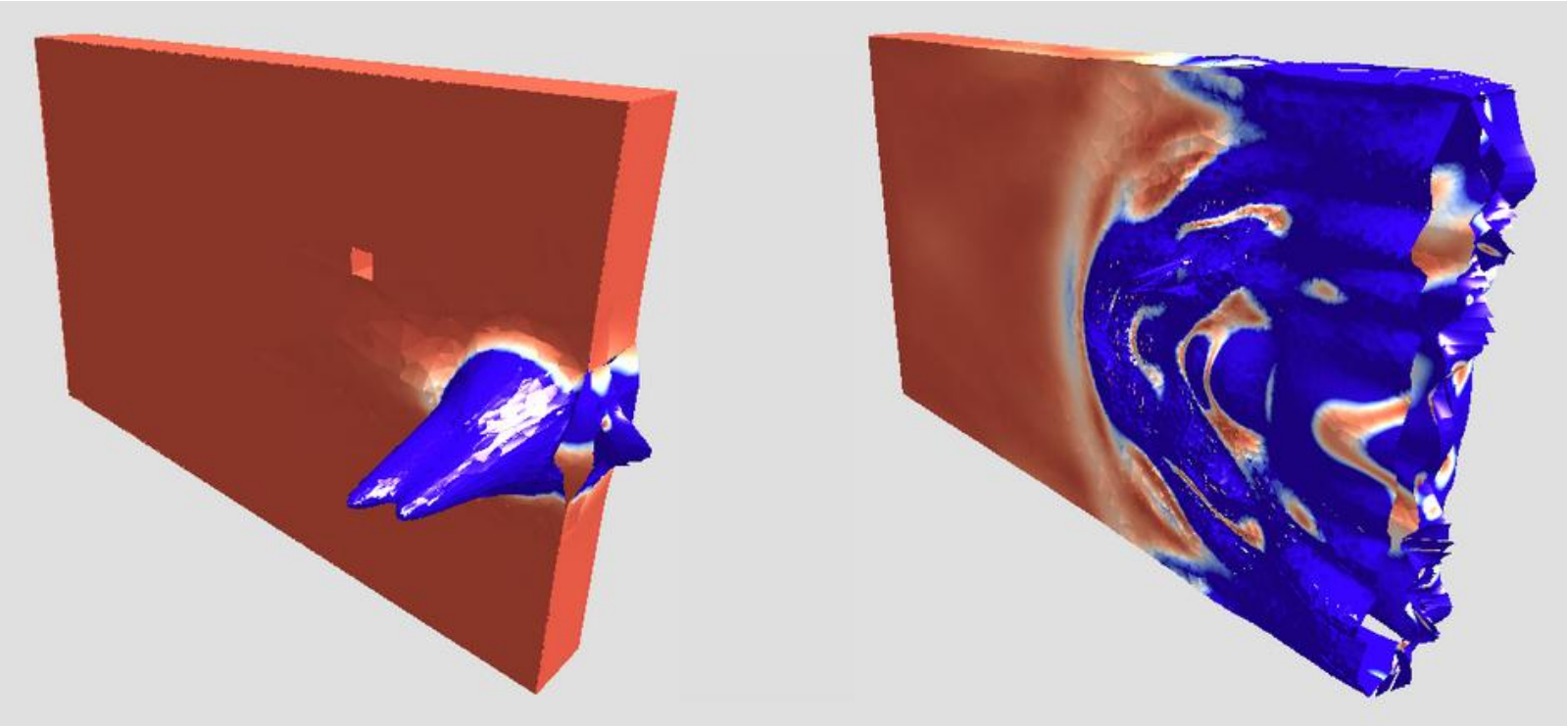

Color: strain energy (blue: high); Height: velocity

Acknowledgments

Robert Haber, Jeff Erickson, Michael Garland, Olivier Allix, Scott Miller, Boris Petrakovici, Alex Mont, Shuo-Heng Chung, Shripad Thite, Yong Fan, Morgan Hawker, Jayandran Palaniappan, Yuan Zhou, Karel Matous